Bhattacherjee, A., Sneha, M., Lewis-Borrell, L. J., Amoruso, G., Oliver, T. A. A., Tyler, J. L., Clark, I. P., & Orr-Ewing, A. J. (2021). Singlet and Triplet Contributions to the Excited-State Activities of Dihydrophenazine, Phenoxazine, and Phenothiazine Organocatalysts Used in Atom Transfer Radical Polymerization. *Journal of the American Chemical Society*, *143*(9), 3613 - 3627. https://doi.org/10.1021/jacs.1c00279

Singlet and Triplet Contributions to the Excited-state Activities of Dihydrophenazine, Phenoxazine and Phenothiazine Organocatalysts used in Atom Transfer Radical Polymerization

Aditi Bhattacherjee[1#*], Mahima Sneha[1#*], Luke Lewis-Borrell[1#], Giordano Amoruso[1], Thomas A.A. Oliver[1], Jasper Tyler[1], Ian P. Clark[2] and Andrew J. Orr-Ewing[1*]

[1] School of Chemistry, University of Bristol, Cantock's Close, Bristol BS8 1TS, UK

[2] Central Laser Facility, Research Complex at Harwell, Science and Technology Facilities Council, Rutherford Appleton Laboratory, Harwell Oxford, Didcot, Oxfordshire, OX11 0QX, UK

Present address for A.B: Department of Chemistry, University of Iowa, Iowa City, Iowa 52242, United States

*Correspondence: A.B. (aditi-bhattacherjee@uiowa.edu), M.S. (mahima.sneha@bristol.ac.uk) and A.J.O.E (a.orr-ewing@bristol.ac.uk)

# Authors contributed equally.

ORCID:

Aditi Bhattacherjee 0000-0001-7146-1128

Mahima Sneha 0000-0003-4896-6915

Luke Lewis-Borrell 0000-0002-6198-722X

Giordano Amoruso 0000-0003-0244-4804

Thomas A.A. Oliver 0000-0003-3979-7857

Jasper Tyler 0000-0002-3155-1847

Andrew J. Orr-Ewing 0000-0001-5551-9609

Abstract

The photochemical dynamics of three classes of organic photoredox catalysts employed in organocatalyzed atom-transfer radical polymerization (O-ATRP) are studied using time-resolved optical transient absorption and fluorescence spectroscopies. The nine catalysts selected for study are examples of N-aryl and core-substituted dihydrophenazine, phenoxazine and phenothiazine compounds with varying propensities for control of polymerization outcomes. Excited singlet state lifetimes extracted from the spectroscopic measurements are reported in N,N-dimethylformamide (DMF), dichloromethane (DCM) and toluene. Ultrafast (< 200 fs to 3 ps) electronic relaxation of the photocatalysts after photoexcitation at near-UV wavelengths (318-390 nm) populates the first singlet excited state (S_1). The S_1-state lifetimes range from 130 ps to 40 ns with considerable dependence on the photocatalyst structure and the solvent. Competition between ground-electronic state recovery and intersystem crossing controls triplet state populations and is a minor pathway in the dihydrophenazine derivatives, but is of greater importance for phenoxazine and phenothiazine catalysts. Comparison of our results with previously reported O-ATRP performances of the various photoredox catalysis shows that high triplet-state quantum yields are not a pre-requisite for controlling polymer dispersity. For example, the 5,10-di(4-cyanophenyl)-5,10-dihydrophenazine photocatalyst, shown previously to exert good polymerization control, possesses the shortest S_1-state lifetime (135 ps in DMF and 180 ps in N,N-dimethylacetamide) among the nine examples reported here, and a negligible triplet state quantum yield. The results call for a re-evaluation of the excited state properties of most significance in governing the photocatalytic behaviour of organic photoredox catalysts in O-ATRP reactions.

1. Introduction

Controlled methods for radical polymerization are of great interest for the synthesis of polymers with a desired molecular weight or chain length. Photoredox-catalysed atom transfer radical polymerization (ATRP), in particular, has emerged as an effective approach for the controlled synthesis of polymers with a precise composition and dispersity.[1] Recent developments in organic photoredox catalysis have improved these radical-based polymerization reactions by, most notably, avoiding contamination from metal-containing catalysts.[2-5] This progress has motivated the development of new classes of organic photocatalyst (PC) molecules based on N-aryl phenothiazines, phenoxazines and dihydrophenazines that have provided the benchmark for organocatalyzed ATRP (denoted O-ATRP).[3, 6-8]

The redox properties of a molecular photoredox catalyst mainly arise from the higher oxidation or reduction potential of the excited singlet or triplet electronic states of the molecule compared to its ground electronic state.[2] Both synthetically and computationally directed strategies for higher efficiency photoredox catalysts are built on accessing excited electronic states with long lifetimes that enable diffusive bimolecular electron transfer reactions with a radical precursor.[9-11] Molecular triplet states are sufficiently long-lived to favour intermolecular single electron transfer to radical initiators over intramolecular deactivation pathways. For this purpose, many early photocatalysts deliberately incorporated transition metal atoms as chromophores to enhance intersystem crossing rates through high spin-orbit coupling.[12]

Seminal research on O-ATRP optimization has placed emphasis on the energy of the lowest-excited triplet state (T_1) of a given photoredox catalyst to predict, rationalize, and tailor photocatalytic activities.[6, 10, 13] This emphasis derives mainly from three premises: (a) spin-forbidden relaxation to the ground state prolongs the lifetime of a triplet state in comparison to a

singlet state;[11] (b) back electron transfer, which quenches photoredox activity, is inhibited in the triplet-spin radical pairs formed by initial electron transfer from the photocatalyst T_1 state (although this is less of a concern for dissociative electron transfer pathways exploited in O-ATRP);[2] (c) organic photocatalyst design should draw on existing knowledge of the photophysical behaviour of organometallic complexes,[12] many of which exhibit ultrafast intersystem crossing (ISC).[14-16] The need for organic PCs to have long excited-state lifetimes has recently been challenged,[17, 18] and we instead propose a greater focus on excited state reduction potentials, regardless of the excited state spin multiplicity, as a controlling factor in O-ATRP optimization because of their influence on intermolecular electron transfer rate coefficients.[17] Consequently, molecules with few nanosecond fluorescence lifetimes and low triplet quantum yields may participate in bimolecular electron transfer reactions driving O-ATRP through their S_1 states instead of their triplet states.

Although organic photocatalysts do not contain metal ions, useful analogies may be drawn between the metal-centred or metal-to-ligand charge transfer (CT) states common in photo-excited metal complexes and the locally excited (LE) or CT-character excited states of organic compounds such as dihydrophenazines, phenoxazines and phenothiazines.[11, 19, 20] This LE vs CT character of the frontier orbitals has been argued to account for large discrepancies in photocatalytic efficiencies of organic compounds that have similar reducing potentials of their triplet states. A LE state descriptor is used when the frontier π and π* orbitals are both localized over the core (a heterocyclic ring fused between two benzene rings, see Figure 1); CT instead describes spatially separated π and π* orbitals that are delocalized over the core and N-aryl groups, respectively. In CT states, electron-withdrawing (donating) groups on the N-aryl rings stabilize (destabilize) the spatially separated π*-SOMOs. This spatial separation between the two SOMO electrons has been

proposed to facilitate ISC and intermolecular electron transfer.[7, 11, 20] Here, we present direct counter-evidence that one such optimized PC (5,10-di(4-cyanophenyl)-5,10-dihydrophenazine) with an electron-withdrawing nitrile (-CN) functionality on the N-aryl group stabilizing its CT-character S_1 and T_1 states repopulates the S_0 ground electronic state two orders of magnitude faster than the corresponding PC (5,10-bis(4-methoxyphenyl)-5,10-dihydrophenazine) with electron-donating substituents (-OMe), which is detrimental to the efficiencies of both ISC and bimolecular electron transfer reactions.

In the current work, we study the solvent-dependent photochemical dynamics of nine PCs based on dihydrophenazine, phenoxazine, and phenothiazine central cores (Figure 1). Such compounds have been widely applied in the recent development of O-ATRP.[3, 6, 21, 22] These prior works characterized the steady-state spectroscopies and excited-state redox potentials of these (and other) organic photocatalysts, the latter by combining cyclic voltammetry data with calculated excited state energies, and tested their polymerization control of the as-grown polymer dispersity.[9, 23-27] Design principles have focused on enhanced absorption of near-ultraviolet or visible light for photoinitiation and radical generation to make these polymerization reactions amenable to activation by light emitting diodes or natural sunlight, and to avoid undesirable side reactions.[6]

The PCs chosen for the current study are shown in Figure 1. They make use of modifications to N-atom and core substituents,[7] and show varying performances in O-ATRP that we seek to understand. The selected PCs are five dihydrophenazine (denoted PC-N), three phenoxazine (PC-O), and one phenothiazine (PC-S) derivatives – note that this nomenclature is used specifically in this work to distinguish between the differing heteroatoms. In four of these cases, (PC-N2, PC-N3, PC-N5, PC-O1), prior publications from our group have reported the analysis of transient absorption spectroscopy data to determine S_1-state lifetimes.[17, 28, 29] New

solvent-dependent fluorescence lifetime measurements are presented here for all nine PCs, together with previously unreported mid-IR and UV-visible transient absorption spectroscopy studies for five of them, in three solvents chosen for their different polarities (Table S1). The selected solvents are N,N-dimethylformamide (DMF), dichloromethane (DCM), and toluene. In addition, for the four previously studied PCs (PC-N2, PC-N3, PC-N5, PC-O1), new mid-IR transient absorption spectroscopy measurements are presented which extend over much greater time intervals than our prior work. The combined outcomes from the current and our prior measurements provide a consolidated picture of the effects of structural modifications and solvent properties on the photodynamics of dihydrophenazine, phenoxazine and phenothiazine PCs.

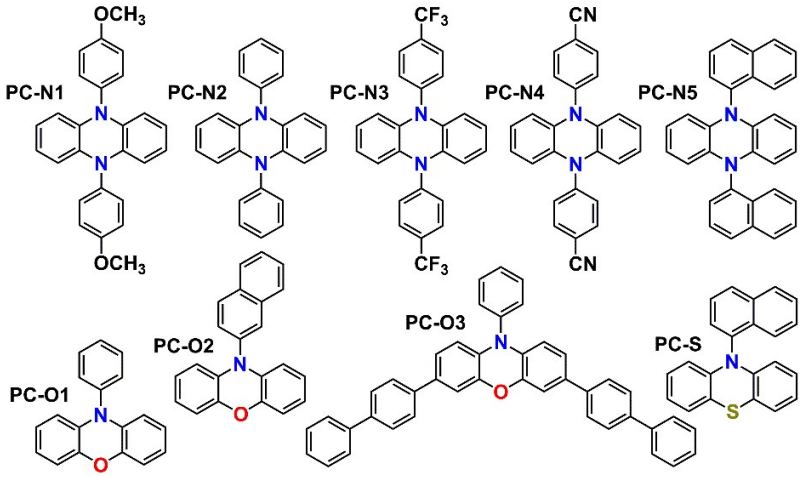

Figure 1: Structures of nine organic photocatalyststs studied here. PC-N, PC-O and PC-S nomenclature indicates dihydrophenzine, phenoxazine, and phenothiazine core structures, respectively. The core heteroatoms are emphasized by coloured labels. The PCs N1 to N5, and O1 to O3 further differ in their N-aryl substituents. Only one phenothiazine catalyst is studied. PC-O3 further incorporates core modification by the addition of biphenyl groups.

The structural modifications in the chosen organic PCs explore the effects of changing one central-ring heteroatom in the core dihydrophenazine, phenoxazine or phenothiazine moiety, and of altering the N-aryl substituents, for example by comparing the effects of either electron donating

or withdrawing groups. In the literature, PC-N3, PC-N4 and PC-N5 are reported to be promising dihydrophenazine-based photocatalyst with high efficiency and polymer dispersity control.[6] PC-O1 and PC-O2 are both effective phenoxazine-based catalysts with a phenyl or naphthyl substituent at the N atom. PC-O3 additionally involves substitution at the phenoxazine core with biphenyl groups, added to enhance visible light absorption via extended conjugation. Finally, PC-S is a phenothiazine-based catalyst representing a class of organic PCs reported to have superior reducing properties than metal-centred PCs, and high ISC quantum yields.[3, 10, 13]

2. Methods

The PCs indicated in Figure 1 were synthesized according to published protocols in the literature,[6, 7, 30] and detailed description of the methods and characterisation can be found in Section S1 of Supporting Information. The solvents N,N-dimethylformamide, dichloromethane, toluene (all anhydrous, ≥99.8%), and toluene-d_8 (99 atom% D) were purchased from Sigma Aldrich and used without further purification. Relevant solvent properties are summarized in Table S1 of Supporting Information.

The time-resolved absorption spectroscopy measurements employed solutions of the PCs in various concentrations, adjusted for the sample pathlength (see below), that were chosen not to exceed an absorbance of 0.5 at the excitation wavelength. Typical concentrations, unless otherwise indicated, were 4.2 mM (PC-N1), 5 mM (PC-N4), 3.2 mM (PC-O1), 2.9 mM (PC-O2), 1 mM (PC-O3), and 7.6 mM (PC-S). To ensure a fresh part of the sample was excited and probed with every laser measurement, the solutions were circulated from a 10-ml sample vial using a peristaltic pump, and sample cells were spatially rastered. For most measurements, samples were not purged by nitrogen because the excited-state dynamics of interest were too rapid to be affected

by dissolved oxygen. However, to assist the assignment of triplet-state contributions to the photochemistry of the PCs, the effects of quenching by oxygen over longer (ns to μs) timescales were tested by comparing with measurements made on samples purged with nitrogen. Even with the use of a sealed flow system reported previously,[28] interference by dissolved oxygen could not be completely suppressed.

a) Transient absorption spectroscopy

Transient electronic absorption spectroscopy (TEAS) was carried out at the University of Bristol using a UV pump pulse (at wavelengths of 370 nm for PC-N1 and PC-N2, 318 nm for PC-O1, PC-O2 and PC-S, 389 nm for PC-O3) and white-light continuum (WLC) probe (340-700 nm) pulse.[31, 32] The WLC was generated by focusing 800-nm pulses into a 3-mm thick CaF_2 window that was rastered both horizontally and vertically to prevent optical damage. The WLC probe was subsequently recollimated by an off-axis parabolic mirror before being focussed and spatially overlapped with the pump beam in a non-collinear geometry at the sample. The sample flowed continuously between two CaF_2 windows separated by 380 μm. The transmitted probe was dispersed in a spectrometer (Andor, Shamrock 163) equipped with a 1024-element photodiode array (Entwicklungsbüro Stresing) to measure the transmitted white light spectra in the presence and absence of the pump pulse. The electronic absorption spectrum of holmium oxide was used to provide a pixel-to-wavelength calibration for the spectrometer. The time delay between the pump and probe pulses was controlled by an optical delay line and limited to a maximum of 1.3 ns for this experimental setup.

Transient vibrational absorption spectroscopy (TVAS) measurements are carried out at the LIFEtime facility (and in a few cases, the ULTRA facility) at the Rutherford Appleton Laboratory.[31, 33-35] These experiments made use of the same pump wavelengths for the various PCs

as indicated for TEAS experiments. However, the mid infrared probe (comprising two separately tunable IR laser pulses, each of ~200 cm^{-1} bandwidth) was tuned to the ring C-C stretch / C-H bend region and spanned 1400 to 1650 cm^{-1}.[17] The linear polarizations of the pump and probe beams were fixed at magic angle (54.7°). After passing through the sample, the probe pulses were dispersed in spectrometers fitted with 128-element MCT (mercury-cadmium-telluride) detector arrays (IR Associates). A pair of CaF_2 windows separated by 100-μm spacers confined the flowing samples. The infrared spectra were wavenumber-calibrated using the known infrared absorption bands of polystyrene. The pump repetition rate was set at 1 kHz and that of the probe was 100 kHz. The pump-probe time delays were continuously tuned from 1 ps to 12 ns using an optical delay line, from 12 ns to 10 μs using electronic delays and probe-pulse selection, and every 10 μs utilizing the 100 kHz repetition rate. The UV pump power was set to deliver a pulse energy of 150 - 300 nJ/pulse at the sample, and the pulse energies of both mid-IR probes were ~0.05 μJ/pulse.

b) Fluorescence lifetime spectroscopy

Sub- and few-ns dynamics in transient absorption spectroscopy measurements were supplemented by time-correlated single photon counting (TCSPC) determinations of photocatalyst fluorescence lifetimes. TCSPC measurements used a custom-built apparatus at the University of Bristol. The fundamental laser output at 680 or 740 nm of a narrowband high power Ti:Sapphire oscillator (3.7 W, 80 MHz, Chameleon Ultra II, Coherent) was frequency-doubled in a 2-mm thick BBO crystal (θ = 29.2°, Eksma), giving excitation wavelengths of 340 or 370 nm. The residual near-IR fundamental light was removed using two dichroic beam splitters (106160, Layertec). To avoid re-excitation of samples, the repetition rate of the laser pulse train was reduced to 3 MHz using an acousto-optic modulator (AOM) based pulse picker (APE cavity dumper kit). Samples were

diluted to have an absorbance of 0.2 at the excitation wavelength, and they were not circulated in TCSPC experiments. The diffracted light from the AOM was subsequently focused through a 10-μm pinhole to remove any undiffracted parent beam, then collimated and focused into the sample with a second lens. Photoluminescence was collected from a 1-cm pathlength cuvette, at 90º relative to the excitation laser, with an infinity-corrected microscope objective (4×/0.2 NA Plan Apochromat, Nikon). The collected fluorescence was filtered to acquire emissions at wavelengths longer than 375 nm or 395 nm (Schott Glass long-pass filter) or 450 nm (long-pass filter FELH0450, Thorlabs) to eliminate laser scatter. A polarizer in the detection line was set to magic angle relative to the excitation laser polarization to remove rotational anisotropy effects from the decay kinetics. The emitted light was focused onto an avalanche-photodiode detector (ID100-20-REG, IDQ) with an achromatic doublet (AC508-075-A, Thorlabs). The photon counts from the detector were acquired by a time-to-digital converter (Time Tagger 20, Swabian Instruments) and binned into histograms with a bin-width of 10 ps. The wavelength dependent instrument response function of the TCSPC spectrometer was determined to be ~170 and 260 ps for 370 and 340 nm excitation, respectively. TCSPC traces were fitted to an analytical solution of a Gaussian instrument response function convoluted with single- or multi-exponential decays.

c) Electronic structure calculations

Computational characterizations of the ground and excited state properties of the PCs were performed using Gaussian 09 software.[36] Geometries and harmonic vibrational frequencies of the ground electronic states of the photocatalysts were computed using restricted Kohn-Sham density functional theory. The pure hybrid-GGA functional PBE0 was used with a polarized and augmented double-zeta basis set 6-31+G(d) (6d,7f). Solvent effects for toluene, DCM and DMF were included by implicit simulation of solvation as a continuous polarizable medium using the

total solute density model (SMD).[37-39] The PBE0 functional long-range London dispersion interactions were simulated with Grimme's D3 dispersion correction, supplemented by the Becke-Johnson damping function (GD3BJ).[40, 41] Vertical transition energies, oscillator strengths and excitation amplitudes were computed with time-dependent density functional theory (TD-DFT) using the Coulomb attenuated variant of the B3LYP functional (CAM-B3LYP).[42, 43] CAM-B3LYP was used with the 6-311++G(2d,p) basis set and non-equilibrium SMD solvation to characterize the excited electronic states of the photocatalyst in the Franck-Condon region.

3. Results and Discussion

Solutions of the organic PCs were first characterized by steady-state absorption and fluorescence spectroscopy. The photochemical dynamics of the PCs were then explored using ultrafast transient absorption spectroscopy, with sub-picosecond time resolution, and time-resolved fluorescence spectroscopy. The time-resolved spectroscopy methods determined excited state lifetimes, propensities for ISC to triplet states, and timescales for recovery of ground-state molecules by a combination of radiative and non-radiative pathways.

a) Steady-state spectroscopy data

The UV-Vis absorption spectra of six of the PCs, measured in DCM, are shown in Figure 2 for wavelengths between 275 and 425 nm, together with the optimized geometries of the PCs in their S_0 states. Corresponding data for the other three dihydrophenazine PCs studied have been reported elsewhere.[17, 28] In their preferred structures, the N-aryl groups of all the PCs are oriented perpendicularly to the central cores to reduce steric repulsion between the H atoms of the aromatic rings. A similar perpendicular orientation is preferred for the biphenyl core substituents in PC-O3. PC-S differs structurally from all other PCs in that it has a puckered phenothiazine core to

accommodate the larger S atom. The UV-vis spectra show that the strongest absorption bands for all PCs lie in the ultraviolet region from 200 to 300 nm; however, we focus here on photoexcitation via the longer wavelength spectral features in view of their applications in visible / near-UV initiated photoredox catalysis.

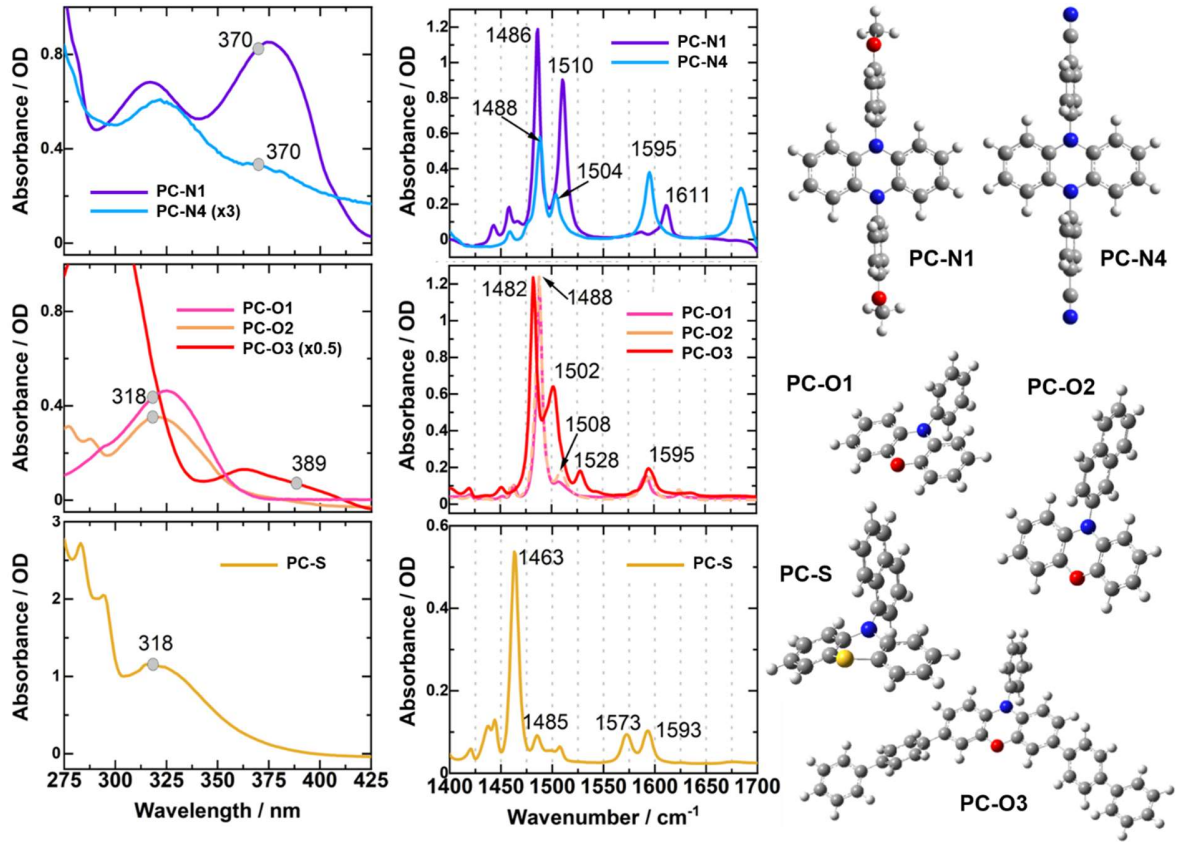

Figure 2: UV-Vis absorption and FTIR spectra of six of the PCs in DCM. Gray circles identify the excitation wavelengths used in the time-resolved spectroscopic investigations. Computed ground-state structures of the organic photocatalysts (PCs) are also shown. The corresponding data for PC-N2, PC-N3 and PC-N5 are reported elsewhere.[17, 28]

The frontier orbitals involved in the long wavelength (>300 nm) photoexcitations of the PCs are predominantly π and π* orbitals. These absorption bands (Figure 2) may consist of multiple, unresolved, $S_0 \rightarrow S_n$ (n = 1 - 4) electronic excitations. Further details of the contributing orbital excitations, oscillator strengths, LE or CT characters of the S_1 states, and S_1 and T_1

reduction potentials are summarized in Table 1. These properties are estimated from computed excited state energies and published ground-state cyclic voltammetry data.[6, 7, 20] The fluorescence emission spectra of all six PCs measured in DMF, DCM, and toluene are shown in Figure S1.

b) Time-resolved spectroscopy of UV-excited photocatalysts

Figure 3 shows the TVAS spectra of six PCs in three different solvents (DMF, DCM, and toluene-d_8). Similar measurements for PC-N2, PC-N3 and PC-N5 are reported elsewhere.[17, 28] The probed IR region from 1400 to 1650 cm^{-1} corresponds mainly to the –C=C– ring stretching / deformation modes of the photocatalysts. For comparison, the FTIR spectra of selected PCs in their ground electronic states in DCM are shown in Figure 2. The presence of strong absorption bands in DMF restricted the observable spectral window for TVAS to 1525 - 1625 cm^{-1} in this solvent. Toluene-d_8 was chosen in place of normal toluene for these experiments because it has fewer interfering infrared features in this region; however, the TEAS and TCSPC experiments made use of normal toluene.

Figure 4 shows the time-dependences of the integrated TVAS band intensities, derived from spectra of the PC solutions in DMF and obtained by fitting the various excited state absorption (ESA) and ground-state bleach (GSB) features to Gaussian functions. The corresponding analyses were also performed for TVAS measurements made with solutions of the PCs in DCM and toluene-d_8. For each combination of a PC and solvent, these types of time-dependent ESA and GSB band intensities were globally fitted to single- or bi-exponential functions to extract the time constants summarized in Tables 2 - 3. The tables also report fluorescence lifetimes for the photoexcited PCs determined from the TCSPC measurements shown in Section S5 of the Supporting Information. Fluorescence lifetimes of a few tens of ns reflect the low

oscillator strengths for the $S_1 \rightarrow S_0$ transitions in some of these photocatalysts (Table 1), whereas significantly shorter fluorescence lifetimes, some of which are sub-ns, indicate competing non-radiative decay pathways from S_1 to S_0 or T_1, or perhaps electron transfer reaction with the solvent in the case of measurements made in DCM.[44]

Table 1: Computed and Experimental Photophysical Data for the Studied PCs in DMF.

Photocatalyst	$S_0 \rightarrow S_n$ wavelength / excitation energy [(a)]	Oscillator strength [(a)]	Reduction potential and electronic LE or CT character [(b)]	
			S_1	T_1
PC-N1	374 nm / 3.3 eV (S_1) 332 nm / 3.7 eV (S_2)	0.0000 0.2056	-2.50 V (LE)	-2.15 V (LE)
PC-N2	376 nm / 3.3 eV (S_1) 333 nm / 3.7 eV (S_2)	0.000 0.206	-2.40 V (LE)	-2.15 V (LE)
PC-N3	374 nm / 3.3 eV (S_1) 337 nm /3.7 eV (S_4)	0.000 0.154	-1.83 V (CT) [(c)]	-2.08 V (CT)
PC-N4	402 nm / 3.1 eV (S_1) 334 nm / 3.7 eV (S_4)	0.0000 0.1508	-2.41 V (CT)	-1.89 V (CT)
PC-N5	377 nm / 3.3 eV (S_1) 314 nm / 3.9 eV (S_4)	0.0024 0.2176	-1.83 V (CT) [(c)]	-1.92 V (CT)
PC-O1	307 nm / 4.0 eV (S_1) 303 nm / 4.1eV (S_2) 290 nm / 4.3 eV (S_3)	0.017 0.056 0.088	-2.44 V (CT)	-2.01 V (CT)
PC-O2	337 nm / 3.7 eV (S_1) 306 nm / 4.1 eV (S_2)	0.0000 0.0303	-1.75 V (CT) [(c)]	-1.76 V (CT)
PC-O3	354 nm / 3.5 eV (S_1) 303 nm / 4.1 eV (S_2)	0.7692 0.3734	-2.02 V (CT)	-1.72 V (CT)
PC-S	320 nm / 3.9 eV (S_1) 308 nm / 4.0 eV (S_2) 282 nm / 4.4 eV (S_3)	0.0018 0.0165 0.0261	-2.16 V (CT)	-1.65 V (CT)

(a) The $S_0 \rightarrow S_n$ photoexcitation wavelengths (nm) and energies (eV), and the corresponding oscillator strengths were computed by TDDFT methods at the CAM-B3LYP/6-311++g(2d,p)/SCRF=(SMD, solvent, NonEq) level of theory.

(b) The reduction potentials (vs SCE) for the S_1 and T_1 excited electronic states were calculated using $E^{e}(PC^{\cdot+}/PC) - E(PC^*)$, where $E(PC^*)$ denotes the energy (in eV) of the S_1 or T_1 state. S_1 energies were estimated from the wavelengths of maxima in experimental emission bands, and T_1 energies were calculated using DFT methods. $E^{e}(PC^{\cdot+}/PC)$ values measured by cyclic voltammetry were taken from Refs. [6, 7, 20]. Locally excited (LE) or charge-transfer (CT) characters of the excited states were deduced from the computed molecular orbitals.

(c) The method of determination of these $E^{e}(PC^{\cdot+}/{}^1PC(S_1))$ appears to underestimate their values.

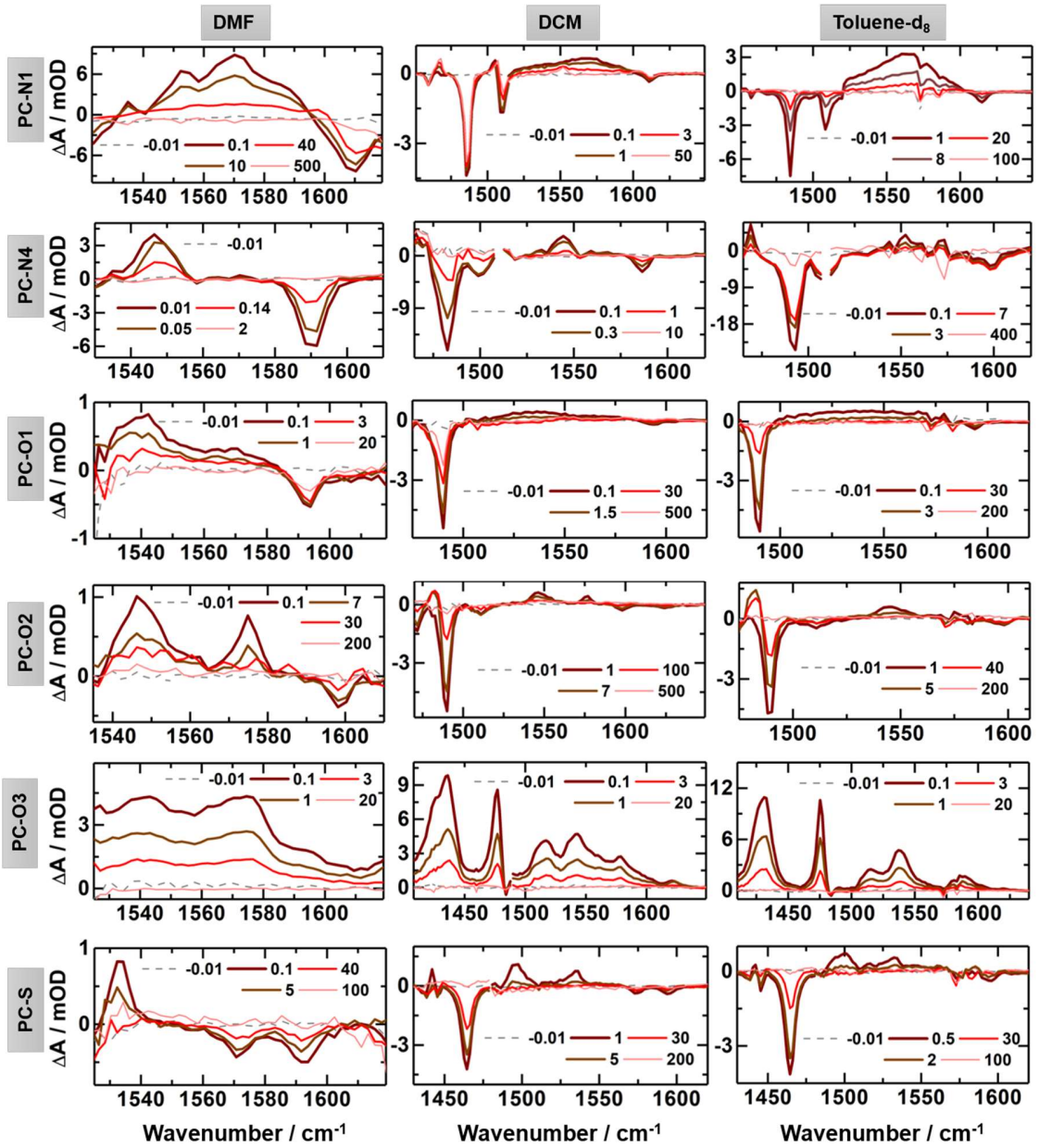

Figure 3: TVAS measurements for six PCs in solution in DMF, DCM, and toluene-d_8, shown at the selected time delays in nanoseconds indicated by the inset keys. In each case, measurements were also made at multiple time delays up to 10 μs (not shown). A negative time trace (-0.01 ns) is shown as a dashed grey line in all the panels to provide a reference for the baseline. The concentrations of the solutions were 4.2 mM (PC-N1), 10 mM (PC-N4), 3.2 mM (PC-O1), 2.9 mM (PC-O2), 1 mM (PC-O3), and 7.5 mM (PC-S). Gaps in the data (PC-N4 in DCM and in toluene-d_8 at 1510 cm^{-1}; PC-O3 in DCM at 1480 cm^{-1}) resulted from damaged pixels in the MCT array detector. A discontinuity in the spectrum for PC-N1 in toluene-d_8 at 1520 cm^{-1} was an artefact of joining two separate MCT detectors. The spectral noise in the TVAS measurements in toluene-d_8 at 1575 and 1585 cm^{-1} was caused by low counts on the detector because of solvent infrared absorption features.

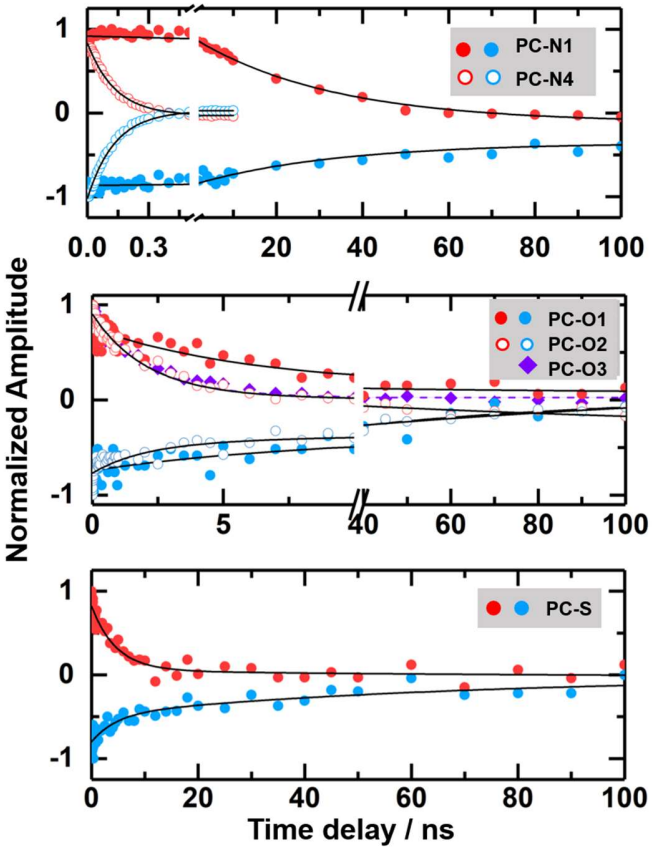

Figure 4: Kinetic traces from TVAS for six UV-photoexcited PCs in DMF obtained by integrating band intensities at different time delays. Positive amplitude traces with red or purple symbols denote excited state absorption (ESA), and negative amplitude traces with blue symbols denote ground state bleaches (GSB). Insets show to which PCs the traces correspond. Note that the magnitudes of all peak amplitudes are normalized to one. For a given PC, the decays of both ESA and GSB intensities were globally fitted (solid black lines) to single or biexponential functions to extract a consistent set of photophysical time constants (see Table 3).

Table 2: Time Constants (in ns) Obtained from the Fitting of Kinetic Data from TVAS and TCSPC Measurements for UV-Photoexcited Dihydrophenazine PCs in Three Solvents, DMF, DCM and Toluene-d_8 (Normal Toluene for TCSPC).

		Time constants from TVAS and TCSPC data / ns [(b)]		
Photocatalyst	**Method [(a)]**	**DMF**	**DCM**	**Toluene-d_8**
PC-N1	TVAS	0.15 ± 0.07 [(c)] 38.5 ± 1.3	0.030 ± 0.004 [(c)] 2.2 ± 0.1[(d)]	0.077 ± 0.007 [(c)] 11.7 ± 0.2
	TCSPC	19.55 ± 0.17	0.30 ± 0.17 [(f)] (43%) 2.30 ± 0.17 [(d)] (57%)	10.95 ± 0.17
PC-N2	TVAS	16.8 ± 2.0 287 ± 21 [(e)]	0.013 ± 0.002[(c)] 2.77 ± 0.40 [(d)] [(g)]	25.5 ± 7.6 104 ± 15 [(e)] [(g)]
	TCSPC	12.98 ± 0.17	0.24 ± 0.17 [(f)] (37%) 2.55 ± 0.17 (63%)	8.83 ± 0.17
PC-N3	TVAS	0.635 ± 0.022	2.85 ± 0.1 970 ± 160 [(e)]	3.07 ± 0.24 36.4 ± 5.7 [(e)]
	TCSPC	0.76 ± 0.17 (94%)	2.62 ± 0.17	3.25 ± 0.17
PC-N4	TVAS	0.135 ± 0.003 [(g)]	0.51 ± 0.03 [(g)]	5.7 ± 0.3 398 ± 16 [(e)]
	TCSPC	0.20 ± 0.17 (58%) 2.58 ± 0.17 (42%)[(h)]	0.72 ± 0.17 (93%)	5.31 ± 0.17
PC-N5	TVAS[(i)]	5.2 ± 0.4	0.060 ± 0.008[(c)] 17 ± 1 500 ± 100[(e)]	25 ± 1
	TCSPC	5.33 ± 0.17	10.85 ± 0.17	6.13 ± 0.17

(a) 370 nm excitation was used for all measurements on dihydrophenazines.
(b) Single or double entries denote time-constants derived from mono and bi-exponential fits, and percentages in parentheses show relative amplitudes of the components for TCSPC data. Quoted uncertainties are from the experimentally determined IRF, with fits to data returning smaller errors.
(c) Time constant corresponds to growth of S_1 population, perhaps with a vibrational cooling component.
(d) S_1 lifetime shortened by reaction with solvent (dichloromethane).
(e) Assigned to T_1 lifetimes and likely to be affected by O_2 quenching.
(f) Suspected to be fluorescence from UV-excitation of ground state $PC^{\cdot+}$ generated in the solution by light-induced ET reaction of $PC(S_1)$ with DCM. Once formed, the $PC^{\cdot+}$ is stable in solution and can absorb the 370 nm pump light.
(g) Data obtained using the ULTRA laser system at the RAL Central Laser Facility.
(h) Fluorescence spectrum shows unusual behaviour in DMF, with an unexplained second decay component.
(i) Time constants from TVAS data were previously reported,[28] and are added here for comparison.

Table 3: Time Constants (in ns) Obtained from the Fitting of Kinetic Data from TVAS and TCSPC Measurements for UV-Photoexcited Phenoxazine and Phenothiazine PCs in Three Solvents, DMF, DCM and Toluene-d_8 (Normal Toluene for TCSPC).

		Time constants from TVAS and TCSPC data / ns [(b)]		
Photocatalyst	**Method [(a)]**	**DMF**	**DCM**	**Toluene-d_8**
PC-O1	TVAS[(g)]	2.1 ± 0.1 46 ± 12 [(d)]	0.02 ± 0.01 [(c)] 1.5 ± 0.2 43 ± 9 [(d)]	0.014 ± 0.002 [(c)] 2.4 ± 0.2 27 ± 2 [(d)(e)]
	TCSPC[(g)]	2.61 ± 0.26 (79%) [(f)]	1.20 ± 0.26 (84%) [(f)]	2.77 ± 0.26
PC-O2	TVAS	0.07 ± 0.04 [(c)] 8.6 ± 1.2 75 ± 13 [(d)]	0.040 ± 0.008 [(c)] 6.4 ± 0.3 112 ± 4 [(d)(h)]	0.035 ± 0.008 [(c)] 2.4 ± 0.3 57 ± 4 [(d)]
	TCSPC	11.59 ± 0.26	6.55 ± 0.26	2.57 ± 0.26
PC-O3	TVAS	0.58 ± 0.18 3.3 ± 0.4	0.25 ± 0.02 2.57 ± 0.05	0.50 ± 0.12 2.4 ± 0.3
	TCSPC	2.72 ± 0.17	2.40 ± 0.17	2.01 ± 0.17
PC-S	TVAS	5.9 ± 0.6 78 ± 30 [(d)]	0.014 ± 0.003 [(c)] 3.8 ± 0.2 395 ± 10 [(d)]	0.007 ± 0.001 [(c)] 1.77 ± 0.08 673 ± 18 [(d)]
	TCSPC	6.27 ± 0.26	3.90 ± 0.26	1.85 ± 0.26

(a) Excitation wavelengths were 318 nm for TVAS and 340 nm for TCSPC, with the exception of PC-O3 which was excited at 389 nm for TVAS and 370 nm for TCSPC.
(b) Single or double entries denote time-constants derived from mono and bi-exponential fits, and percentages in parentheses show relative amplitudes of the components for TCSPC data. Quoted uncertainties are from the experimentally determined IRF, with fits to data returning smaller errors.
(c) Time constant corresponds to growth of S_1 population, perhaps with a vibrational cooling component.
(d) Assigned to T_1 lifetimes and likely to be affected by O_2 quenching.
(e) Extends to 840 ± 31 ns with improved N_2 purging.
(f) Minor contributions from a second time constant of 6.78 ± 0.26 ns in DMF and 6.10 ± 0.26 ns in DCM are also observed in the TCSPC experiments.
(g) Time constants for PC-O1 were previously reported from our laboratory,[29] and are added here for comparison.
(h) Extends to 1.63 ± 0.03 μs with improved N_2 purging.

Complementary TEAS measurements for DMF, DCM and toluene solutions of the PCs are shown in Figure 5. The methods for spectral decomposition into S_n, S_1 and T_1 ESA bands, performed using the KOALA program,[45] are reported in Section S4 of the Supporting Information. Kinetic fitting of the time-dependent intensities of the spectral components gave the exponential time constants summarized in Table 4. The following discussion considers in turn the

photodynamics of the dihydrophenazine, phenoxazine and phenothiazine PCs deduced from all the excited-state population growth and decay time constants summarized in Tables 2 - 4.

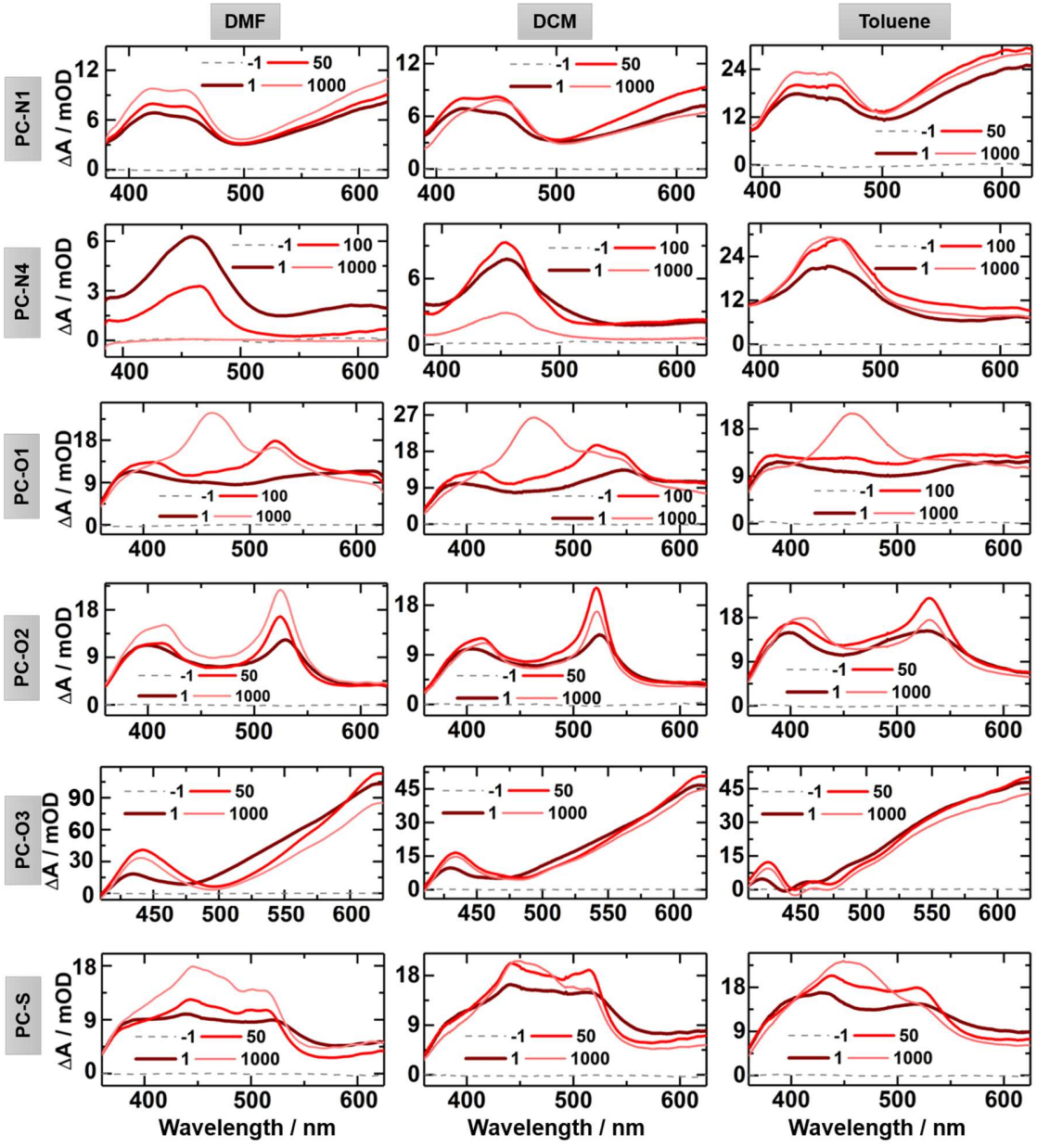

Figure 5: Transient electronic absorption spectra measured for six PCs in DMF, DCM and toluene up to a maximum time interval of 1 ns. The legend indicates representative pump-probe time-delays in picoseconds. The solid grey line (-1 ps, where the probe pulse arrives at the sample before the pump pulse) provides a reference for the baseline. Figure S3 of the Supporting Information further shows TEAS data measured in DMAc.

Table 4: Exponential Time-Constants for Growth and Decay of Bands in the TEAS Spectra of the Dihydrophenazine, Phenoxazine and Phenothiazine PCs in DMF, DCM and Toluene Solutions.

	Time constants / ps [(a) (b) (c)]		
Photocatalyst	**DMF**	**DCM**	**Toluene**
PC-N1	2.8 ± 0.4 (↑ S_1) 134 ± 12 (↑ S_1)	30 ± 4 (↑ S_1) 2200 ± 100 (↓ S_1)	2.7 ± 0.6 (↑ S_1) 54 ± 6 (↑ S_1)
PC-N2	13 ± 2 (↑ S_1) [(d)]	18 ± 3 (↑ S_1) ~2770 (↓ S_1, ↑ T_1)	23 ± 2 (↑ S_1)
PC-N3	613 ± 54	0.400 ± 0.01(↑ S_1) 31.0 ± 5.0 (↑ S_1)	1.7 ± 0.1 (↑ S_1) ~3000 (↓ S_1, ↑ T_1)
PC-N4	2.4 ± 0.2 (↑ S_1) 136 ± 9 (↓ S_1)	1.1 ± 0.1 (↑ S_1) 18.4 ± 1.6 (↑ S_1) ~510(↓S_1)	1.0 ± 0.1 (↑ S_1) 17.7 ± 1.4 (↑ S_1)
PC-N5	10.4 ± 2.6 (↑ S_1) 111 ± 8 (↑ S_1)	3.4 ± 0.7 (↑ S_1) 54.6 ± 3.3 (↑ S_1)	4.7 ± 0.3 (↑ S_1) 91 ± 5 (↑ S_1)
PC-O1	14.8 ± 0.3 (↑ S_1) 2100 ± 100 (↓ S_1, ↑ T_1)	14.8 ± 0.4 (↑ S_1) 1500 ± 200 (↓ S_1, ↑ T_1)	22.8 ± 1.0 (↑ S_1) 2400 ± 200 (↓ S_1, ↑ T_1)
PC-O2	1.9 ± 0.2(↑ S_1) 77 ± 6(↑ S_1) ~8600(↓ S_1, ↑ T_1)	0.60 ± 0.01(↑ S_1) 20 ± 0.5(↑ S_1) ~6400(↓ S_1, ↑ T_1)	2.1 ± 0.1(↑ S_1) 21.0 ± 1.5 (↑ S_1) ~2400(↓ S_1, ↑ T_1)
PC-O3	2.9 ± 0.1 (↑ S_1) ≥ 2500 (↓ S_1)	250 (↑ S_1) 2400 (↓ S_1)	500 (↑ S_1) 2400 (↓ S_1)
PC-S	1.4 ± 0.1 (↑ S_1) 51.0±5.2 (↑ S_1) 4900 (↓ S_1, ↑ T_1)	0.9 ± 0.1 (↑ S_1) 21 ± 2 (↑ S_1) ~3900 (↓ S_1, ↑ T_1)	2.0 ± 0.1(↑ S_1) 19.4 ± 3.2(↑ S_1) ~1770(↓ S_1, ↑ T_1)

(a) The symbols ↑ and ↓ denote growth and decay, respectively, of the intensities of ESA bands assigned to the specified states.
(b) Recovery of S_0 population may be biexponential, but always shows one time constant in agreement with S_1 population decay.
(c) Time constants greater than 1000 ps are poorly determined from fits to the TEAS measurements which extend only to 1.3 ns. Instead, time constants from TVAS (Tables 2 and 3) were shown to be consistent with the TEAS data.
(c) Value obtained in DMAc.

i) Dihydrophenazine Catalysts

PC-N1 and PC-N4 are examples of dihydrophenazine catalysts with electron-donating (-OMe, PC-N1) and electron withdrawing (-CN, PC-N4) N-phenyl para-substituents, and are chosen as the focus of the discussion because of these contrasting electronic properties. Where

appropriate, further comparisons are drawn with the other dihydrophenazine PCs studied. The triplet excited-state reduction potentials, $E^{o}(PC^{\cdot+}/^{3}PC^{*})$, of PC-N1 and PC-N4, obtained by combining DFT calculations of excitation energies and ground-state redox potentials (versus saturated calomel electrode) are -2.15 V and -1.89 V, respectively.[6] These values are compared with the corresponding estimates for the S_1-state reduction potentials in Table 1. Without any N-phenyl substituents (i.e., PC-N2), the corresponding T_1-state reduction potential is -2.15 V. All these dihydrophenazine derivatives are more reducing from their T_1 states (and by implication, their S_1 states) than commonly used metal-centred PCs such as polypyridyl iridium complexes following photoexcitation.[12]

The electron-withdrawing substituents stabilize excited states of CT character and lower their reduction potentials compared to states with LE character. In these ππ* CT states, the electron density in the lower-lying π-SOMO is mainly on the dihydrophenazine core whereas that in the higher π*-SOMO is mainly on the N-phenyl ring(s). This delocalization is augmented by -CN (in PC-N4) or $-CF_3$ (in PC-N3) groups in the para position. Miyake and co-workers hypothesized that the superior photocatalytic ATRP performances of PC-N4 and PC-N3 in comparison to PC-N1 derives from their excited-state CT character, and used this principle as the basis for further PC design.[6, 20] Our quantification of the effects of the N-phenyl ring substituents, and hence of the CT or LE character of the T_1 (or S_1) states, on the rate coefficients for intermolecular electron transfer reactions that initiate an ATRP cycle is the subject of a forthcoming publication.

The TDDFT calculations indicate that photoexcitation is to the S_2 state in PC-N1 and the S_4 state in PC-N4 at the near-UV wavelengths used here. Internal conversion to S_1 proceeds on ultrafast timescales, faster than intermolecular electron-transfer reactions or radiative decay, in accordance with Kasha's rule.[46] This ultrafast relaxation $S_n \rightarrow S_1$ is mostly comparable to, or faster

than, the temporal resolution of our TVAS experiments, but can be observed by this spectroscopic method in the case of PC-N1 as a combination of internal conversion and vibrational cooling kinetics (see Tables 2 and 4).

When photoexcited at 370 nm, PC-N1 shows strong, moderate, and weak GSB features at 1485, 1511, and 1613 cm^{-1}, respectively, in the TVAS spectra of Figure 3. In contrast to these sharp depletion bands, which have 5 to 10 cm^{-1} full-widths-at-half-maximum (FWHM), the feature due to ESA is unusually broad, spanning from 1530 to 1590 cm^{-1}. This width is likely to derive from overlapping vibrational bands of the S_1 state (as discussed below and in Section (c), there is no clear evidence for T_1 population in our data for PC-N1). In comparison, PC-N4 shows one strong and two weak GSB features at 1488, 1503, and 1595 cm^{-1}, respectively, when photoexcited at 370 nm. An observed ESA band at 1547 cm^{-1} is much narrower than for PC-N1; for PC-N4, all peaks have a width of 15 to 20 cm^{-1}. The ground-state FTIR spectral absorptions in this region match the wavenumbers of the GSB features and have a FWHM of 10 cm^{-1}, which is ascribed to inhomogeneous broadening by interaction with the solvent (see Section S3 of Supporting Information for steady state FTIR spectra).

N,N-dimethylacetamide (DMAc) is the solvent medium used in several reported O-ATRP photopolymerization studies. Of the three solvents used here, DMF most closely resembles DMAc in terms of polarity (Table S1), and it is a useful analogue because the IR spectrum of DMAc masks all the transient absorption features of interest. Inspection of Figures 3 and 4 shows that all the spectral features described above which fall in the narrow IR-transparent window of DMF decay completely to zero. However, ground-state recovery is much faster for PC-N4 than PC-N1. Reasonable agreement between time constants deduced from the analysis of TVAS and TCSPC data (Table 2) confirms a faster decay of S_1 population in PC-N4. The recovery of the GSB mirrors

the decay of the ESA, which indicates a predominantly direct relaxation pathway from the S_1 to the S_0 state without significant involvement of any intermediate electronic state (e.g., T_1).

Both prior and the current measurements for DMF solutions of PC-N3, which has para, electron-withdrawing -CF_3 substituents on the N-phenyl groups, show fast (~700 ps) internal conversion to the ground state, on timescale approaching that for PC-N4 relaxation.[17] Based on this observation, we posit that the polar solvent apparently stabilizes the CT-character S_1 states of PC-N4 and PC-N3, thereby reducing the S_1-S_0 energy gap and opening up a rapid internal conversion (IC) route to S_0 (most likely through a conical intersection), which outcompetes fluorescence decay or ISC. Such pathways are not accessible for the LE-character S_1 state of PC-N1, nor for PC-N2 studied both here and previously by Koyama *et al.*[17] The S_1 excited-state lifetime for PC-N4 in DMF was independently verified using TEAS to be 136 ± 9 ps (*c.f.* 135 ps by TVAS), following a 2.4 ± 0.2 ps growth by IC from the photoexcited S_4 state. The experimentally determined S_1 lifetime for PC-N4 in DMAc was found to be ~180 ps by TEAS, consistent with expectations based on the similar polarities of the two solvents. Thus, for PC-N4 and PC-N3, both of which have been shown to provide good dispersity control in the polymer products of O-ATRP, we find that the excited state lifetime is shorter than nanosecond timescales for diffusional bimolecular electron transfer reactions at the concentrations used in O-ATRP synthesis.

In DCM, PC-N4 ground state recovery is also complete (Figure 3), and the timescale matches that of the decay of the S_1 ESA bands observed by TVAS, indicating little or no branching into the triplet manifold by ISC. Comparison of the time constants in Tables 2 and 4 shows that the relaxation dynamics in DCM (510 ± 30 ps) are comparable to those in DMF (135 ± 3 ps). In toluene, however, PC-N4 behaves differently: while the S_1 ESA decays with a time constant of 5.7

± 0.3 ns, the ground state bleach shows a biexponential recovery with time constants of 5.7 ± 0.3 ns and 398 ± 16 ns. We assign this second time constant to the quenching of T_1-state population by dissolved oxygen, details of which are discussed in Section 3(c). The longer S_1 lifetime in toluene is supported by our TCSPC data, and by observation of strong fluorescent emission from PC-N4 in this solvent, but not in DMF or DCM under the same measurement conditions. TEAS measurements show that the main S_1 ESA band of PC-N4 centred at 450 nm grows with 1.0 ± 0.1 ps and 17.7 ± 1.4 ps time constants in toluene (and 1.1 ± 0.1 ps and 18.4 ± 1.6 ps in DCM) which we attributed to IC and vibrational cooling in the S_1 state, respectively. A shift of the band maximum to shorter wavelength at times longer than 5 ps is consistent with this latter interpretation.

For PC-N1 in toluene-d_8, TVAS measurements show that the ground-state recovery is complete within 100 ns. The time constant for the decay (11.7 ± 0.6 ns) matches that obtained from TCSPC (10.95 ± 0.17 ns), and in DMF the ground-state recovery is even slower (time constants of 38.5 ± 1.3 ns from TVAS, 19.55 ± 0.17 ns from TCSPC, with unclear reasons for the discrepancy in the values). However, in DCM the photophysical behaviour is noticeably different, with an ESA decay time constant of 2.2 ± 0.1 ns. Although the ESA bands assigned to photoexcited PC-N1 in DCM decay completely to zero, the GSB recovery remains 70% incomplete at time delays up to 10 μs, indicating a long-lived intermediate state or reactive loss. Four small positive differential absorbance peaks are noted at 1466, 1508, 1552 and 1601 cm^{-1}, and we assign these bands to the PC-N1$^{\cdot+}$ radical cation, pointing to an electron transfer reaction of the photoexcited PC-N1 with the DCM solvent. This interpretation is consistent with prior reports of halogenated solvents such as DCM participating in electron transfer reactions with photoexcited organic molecules.[44] No such indications of cation formation are seen for

photoexcited PC-N4 in DCM, most likely because the sub-ns relaxation to S_0 (Table 3) outcompetes intermolecular electron transfer to the solvent.

The extended timescale TVAS measurements performed in this work also reveal PC-N2 behaviour that is similar to PC-N1 in the three solvents studied. In DMF and toluene-d_8 solutions, the PC-N2 S_1-state population decays with time constants of 16.8 ± 2.0 ns, and 25.5 ± 7.6 ns respectively, whereas in DCM, PC-N2 has a shorter S_1 lifetime and incomplete ground-state recovery indicating a reaction with the solvent. Both PC-N1 and PC-N2 have LE character in their S_1 states, and the large S_1-state reduction potentials can drive ET reactions with the chlorinated solvent. However, for PC-N2 solutions in DMF and toluene-d_8, the GSB recovery includes a second, slower component with a time constant of ~100-300 ns which we assign to quenching of T_1-state population by dissolved oxygen.

The TEAS data for PC-N1 shown in Figure 5 for solutions in DMF confirm the kinetics of excited state relaxation derived from the TVAS measurements. The observed bands are assigned to S_1 ESA, and spectral decomposition and kinetic analysis give time constants for the growth of this ESA as 2.8 ± 0.4 ps and 134 ± 12 ps. The two time constant values most likely represent steps of internal conversion to S_1 from the initially photoexcited S_2 state and subsequent vibrational cooling in S_1, but a component of direct excitation to the S_1 state followed by vibrational relaxation cannot be discounted. Although formally an electronically forbidden transition (Table 1), the $S_0 \rightarrow S_1$ excitation might become weakly allowed by vibronic coupling. In toluene, the corresponding time constants for growth of the S_1 absorption are 2.7 ± 0.6 ps and 54 ± 6 ps; the latter time constant is also obtained from TVAS band intensity analysis (Table 3). We again interpret these processes as signatures of IC from the photoexcited S_2 state and vibrational relaxation of internally hot PC-N1(S_1) molecules. In DCM, the PC-N1 S_1 population growth with time constant of 30 ± 4 ps is

indicative of $S_2 \rightarrow S_1$ internal conversion and vibrational cooling in S_1. The rate of S_1 population loss is consistent with TVAS measurements, with a time constant of 2.2 ± 0.1 ns. A band consistent with PC-N1$\cdot^+$ production grows on this same timescale, providing further evidence for charge transfer from the PC-N1 S_1-state to the solvent DCM competing with relaxation to S_0.

On the 1.3 ns timescales of the TEAS measurements in DMF and toluene, there is no evidence for the growth of additional features that might correspond to ESA from the T_1 states of the dihydrophenazine PCs PC-N1 and PC-N4. Similar conclusions were drawn in our prior studies of PC-N3 and PC-N5,[17, 28] although spectroscopic evidence for some branching into T_1 was reported for PC-N2 in both DMF and DCM solutions,[17] and is discussed further in Section 3(c).

An interesting trend emerges when we compare the five dihydrophenazine PCs for solutions in DMF: the PCs with CT excited-state character have shorter S_1-state lifetimes - PC-N3 (136 ps), PC-N4 (500 ps) and PC-N5 (5 ns) - than the PCs with LE character - PC-N1 (11 ns) and PC-N2 (17 ns). These observations may hold clues to the S_1-state relaxation mechanisms, but further theoretical work is required to identify the details of the decay pathways.

ii) Phenoxazine Catalysts

The photophysical studies of PC-O1 and PC-O2 use excitation at 318 nm whereas that of PC-O3 is at 389 nm. These excitation wavelengths are chosen because they lie close to the maxima of the first strong absorption bands of the respective molecules in their ground states (Figure 2). Note that these excitation wavelengths are at much shorter (~50 nm, PC-O2, PC-O1) or longer (~19 nm, PC-O3) wavelength respectively than the absorption maxima of the dihydrophenazines discussed above. Consequently, PC-O3 is deemed a more promising visible-light-mediated photoredox catalyst than PC-O1 and PC-O2. Three close-lying excited singlet states of LE and CT

character underly the 280 – 360 nm absorption band in PC-O1 (Table 1).[29] Our previous analysis of PC-O1 showed that the ordering of these states is sensitive to solvent polarity, and that at our excitation wavelength, this PC is predominantly excited to an S_3 state of LE character in DCM or DMF, but to both S_2 (LE) and S_3 (CT) states in toluene.[29] For PC-O2, the calculations reported in Table 1 suggest our 318-nm laser excitation populates the S_2 state which has mixed LE/CT character.

In PC-O3, which was designed to have an absorption spectrum that extends into the visible region, the direct $S_0 \rightarrow S_1$ transition at wavelengths approaching 400 nm (Table 1) involves electronic excitation from a HOMO orbital localized on the phenoxazine core to a SOMO orbital delocalized across the core and both biphenyl substituents. The emissive singlet state was assigned by Sartor *et al*. as having symmetry-breaking CT character involving electron density redistribution from the core to one core-attached biphenyl group (denoted CT-Biphenyl).[11, 24]

TVAS measurements of all the phenoxazine PCs (Figure 3) show a ground-state depletion feature near 1487 cm^{-1}. However, in the case of PC-O3 it is barely discernible against pronounced ESA bands, although the asymmetry in the 1475-cm^{-1} peak is a consequence of the overlapping GSB on the higher wavenumber side. For PC-O1 and PC-O2, the 1487 cm^{-1} GSB feature is both strong and sharp. A second weak GSB band is observed near 1600 cm^{-1} for both PC-O1 and PC-O2, and a third such feature at 1508 cm^{-1} is only seen for PC-O2. On timescales of a few ns, the GSB recovery is incomplete for PC-O1 and PC-O2. Although this ground-state recovery appears complete for PC-O3 within 2 - 3 ns, the extent is difficult to quantify because of the spectral overlap by the numerous ESA features. These observations suggest ISC to the triplet manifold plays a role in S_1 relaxation in PC-O1 and PC-O2, but it is less important for PC-O3. Estimates of ISC quantum yields and rate coefficients are reported in Section 3(c).

Only two weak ESA bands at 1547 and 1575 cm^{-1} are observed for PC-O2 in DMF and DCM. In toluene-d_8, the latter peak is obscured by a solvent band. For PC-O1, we find a broad and weak ESA feature lying between 1500 and 1575 cm^{-1}, the assignment of which is addressed in detail elsewhere.[29] Only the higher wavenumber tail of this absorption band is observed in DMF. For both PC-O1 and PC-O2, we see evidence of a fast initial growth of S_1 absorption bands over a few picoseconds, as reported in Table 3, which we attribute to a combination of internal conversion from the initially photoexcited singlet state and vibrational relaxation in the S_1 state. A band at 1484 cm^{-1} in the TVAS spectra of PC-O2 in DCM grows at later times and is interpreted as a signature of population of the T_1 state on the basis of computed T_1 absorption band frequencies, and because of the observed sensitivity of its decay rate to dissolved O_2.

Figures 3 and 4 show that in DMF solutions, the IR ESA and GSB spectral signatures decay with biexponential behaviour for PC-O1 and PC-O2, but the ESA decay is mono-exponential in PC-O3, with a time constant of 3.3 ± 0.4 ns. The biexponential decay behaviour for PC-O2 persists in DCM and toluene: the faster components (8.6 ± 1.2 ns, 6.4 ± 0.3 ns, and 2.4 ± 0.3 ns in DMF, DCM, and toluene-d_8, respectively) are consistent with TCSPC measurements and correspond to the loss of S_1 population. The larger time constant values are found to be sensitive to N_2 purging of the solutions, which suggests that these correspond to triplet-state lifetimes, and possible overlap of the T_1 and S_1 ESA features in the spectra. Similar considerations apply to PC-O1 in the three solvents, with evidence of S_1 and T_1 states participating in the photodynamics. For PC-O1 in toluene-d_8, we recently estimated a T_1 quantum yield of $\Phi(T_1) = 0.56 \pm 0.03$.[29] We also observed reaction of photoexcited PC-O1 with DCM.

The photodynamics for PC-O3 are broadly consistent for all three solvents, with the decay time-constants showing modest shifts from 2.4 to 3.3 ns. Agreement with time constants from

TCSPC measurements confirms assignment to S_1 population decay, and the measured fluorescence lifetime of 2.72 ns in DMF agrees well with a prior TCSPC study of PC-O3 in DMAc for which a time-constant of 2.87 ns was reported.[24] The features observed by TVAS all decay to baseline within 10 ns, suggesting ISC to the manifold of triplet states is inoperative or at most plays a minor role.

Loss of population from the PC-O1 S_1 state and contributions to the photodynamics from ISC are confirmed by distinct bands observed in the time-resolved electronic spectra (Figure 5). The TEAS spectrum of PC-O1 in DMF clearly shows an intermediate triplet state developing on a nanosecond timescale, as the band assigned to S_1 initially grows and then decays.[29] The early time growth of the S_1 ESA feature (with time constant 14.8 ± 0.3 ps) is attributed to internal conversion after photoexcitation to a higher lying singlet state. Similar photodynamics are observed in the TEAS spectra of PC-O1 in DCM and in toluene. For PC-O2 in toluene and DMF, while a triplet state feature is not as readily discernible as for PC-O1, the later time TEAS traces can be decomposed into a broad S_1 band and a T_1 band centred at 415 nm (Figure S6). However, for PC-O2 in DCM or PC-O3 in all solvents, no new time-dependent ESA peaks are seen in the TEAS spectra up to 1.3 ns. Instead, the changes involved are more subtle and relate to evolution in the peak shapes alone.

The TEAS spectra for PC-O3 are similar to those reported previously, with the prior PC-O3 study conducted in DMAc;[11, 29] the bands of photoexcited PC-O3 observed with centres at 440 nm and 625 nm are assigned to ESA from the S_1 CT-biphenyl state. Our observations of PC-O3 show rapid growth of these ESA features, with associated decay of a shoulder to the 625 nm band located around 540 nm (Figure S4 of Supporting Information). These changes occur with a time constant τ = 2.9 ± 0.1 ps in DMF. We attribute the changing band shapes to vibrational cooling

from the Franck-Condon region of the directly photoexcited S_1 state. The bands then decay with a ≥ 2.5 ns time constant that is consistent with TVAS and TCSPC data (Table 3). In DCM and toluene solutions, the TEAS measurements indicate similar changes to the shapes of the S_1 ESA bands over a few ps (although the evolution of the shoulder on the 625-nm band is less pronounced in toluene) before decay with ~2.4 ns time constants, suggesting similar photodynamics to the DMF solution. Prior to this decay, there may be a small component of growth (or spectral band shift) with 250 – 500 ps time constant, also observed by TVAS (Tables 3 and 4). Sartor *et al*. reported an intersystem crossing quantum yield for PC-O3 in DMAc of $\Phi_{ISC} = 0.11$, involving singlet and triplet states both with CT-Biphenyl character.[24] Our spectroscopic data show no clear evidence for a triplet intermediate state in the three solvents studied.

iii) Phenothiazine Catalyst

PC-S is a phenothiazine catalyst that possesses a puckered central ring.[47] There are conflicting views about the excited state(s) responsible for the photoredox reactivity of phenothiazine PCs, with prior studies pointing to either the short-lived singlet state or the much longer-lived triplet state.[13, 48] At our chosen excitation wavelength of 318 nm, it is likely we excite the S_2 state of PC-S (Table 1) with a weaker contribution from the $S_0 \rightarrow S_1$ transition, and perhaps also from the $S_0 \rightarrow S_3$ transition computed to lie at higher energy.

The TVAS spectra of PC-S (Figure 3), photoexcited at 318 nm in DCM or toluene-d_8, show a strong GSB feature at 1463 cm^{-1} corresponding to depletion of ground-state population, and two weak GSBs at 1573 cm^{-1} and 1591 cm^{-1}. Only the latter two depletions are observed in DMF, with the other masked by strong solvent absorption. ESA bands are evident for PC-S solutions in DCM and toluene-d_8 near 1500 and 1530 cm^{-1} which decay completely to zero within a few tens of

nanoseconds. In DMF, only the higher energy ESA feature can be resolved and decays to zero within 40 ns after photoexcitation.

Time constants extracted from kinetic fits to TVAS data (Table 3) show S_1 relaxation with time constants of 5.9 ± 0.6 ns, 3.8 ± 0.2 ns, and 1.77 ± 0.08 ns in DMF, DCM, and toluene-d_8, respectively. This interpretation is confirmed by TCSPC measurements of fluorescence lifetimes (Table 3), and by a prior report of a singlet state lifetime for PC-S of 7.6 ns in 3-methylpentane at 298 K.[48] The second, slower time components observed in GSB recovery kinetics in all three solvents indicate quenching of T_1-state population, most likely accelerated by dissolved O_2 in the samples.

The TEAS data for PC-S in DMF (Figure 5) show three broad and overlapping peaks, with continued growth of some components up to the longest measured delay time of 1.3 ns. In DCM, the spectra are best described by a decaying exponent with time constant 0.9 ± 0.1 ps, an intermediate with two time constants (0.9 ± 0.1 ps and 21 ± 2 ps) for growth, which then decays as a third Gaussian band centred at 460 nm grows in with a ~ 3.9 ns time constant. The kinetics of the intermediate component are in reasonable agreement with the 14 ± 3 ps growth and 3.8 ± 0.2 ns decay time constant for PC-S (S_1) ESA bands observed by TVAS (Table 3), and this feature is therefore assigned to ESA from the S_1 state. Initial population of S_1 is by internal conversion from the optically excited S_n states, and the band emerging at later times and centred near 460 nm is likely to correspond to ESA from the T_1 state of PC-S, populated by ISC from S_1. Similar behaviour is observed for PC-S in toluene, with a T_1 absorption band centred at 460 nm (Figure 5). This band grows as the broad intermediate S_1 ESA band decays, albeit faster than in DCM, with a time constant of 1.77 ns. Further analysis of the kinetics of ISC in PC-S is presented in the following section.

c) Triplet state branching

Where we have spectroscopic evidence for triplet state population in the various PCs studied, either from distinct absorption bands in the TEAS measurements or from biexponential kinetics for GSB recovery, we deduce rate-coefficients for ISC and the triplet-state branching from the S_1 state in competition with relaxation to S_0. The T_1-state lifetime can be several hundred microseconds.[11] In such a case, we expect the PC ground-state depletion not to recover completely on a ns-to-μs timescale. However, T_1 populations are quenched more rapidly by small amounts of dissolved O_2, which happened to be persistent in our sample flow system even in solutions purged by N_2. Under these conditions, the T_1 lifetimes shortened to tens of nanoseconds or longer. Another contributing factor towards partial or incomplete recovery of the ground state could be reaction from the photoexcited state, for example by electron transfer to a solvent molecule, and we see evidence for this in some of the experiments conducted in DCM, as discussed earlier. Here, the observed amplitudes of components of biexponential or triexponential ground-state recovery in the TVAS experiments are used to guide determinations of an upper limit for the branching into triplet states. For example, for a biexponential GSB recovery with amplitudes of the faster (S_1 decay) and slower (T_1 decay) components denoted by A_1 and A_2 respectively, we estimate the T_1 quantum yield from $\Phi_{ISC} = A_2/(A_1 + A_2)$. Uncertainties in Φ_{ISC} are obtained by appropriate propagation of the fit uncertainties in A_1 and A_2 values. Our analysis assumes that any dissolved O_2 does not influence the rates of ISC or S_1 quenching to S_0. Table 5 summarizes the resulting quantum yields (Φ_{ISC}) and rate coefficients (k_{ISC}) for ISC in the PC solutions studied. The latter values are evaluated using $k_{ISC} = \Phi_{ISC}/\tau(S_1)$ where $\tau(S_1)$ is the measured S_1-state lifetime (Tables 2-3).

Table 5: Estimated Intersystem Crossing Quantum Yields, Φ_{ISC}, and Rate Coefficients, k_{ISC}, Derived from Ground-State Bleach Recovery Kinetics Measured by TVAS. [(a), (b)]

Photocatalyst	S_1 and T_1 character		Solvent		
			DMF	DCM	Toluene-d_8
PC-N1	LE	Φ_{ISC}	–	–	–
		k_{ISC} / 10^8 s^{-1}	–	–	–
PC-N2	LE	Φ_{ISC}	0.71 ± 0.03	–	0.82 ± 0.16
		k_{ISC} / 10^8 s^{-1}	0.42 ± 0.06	–	2.7 ± 0.6
PC-N3	CT	Φ_{ISC}	–	0.19 ± 0.01	0.60 ± 0.06
		k_{ISC} / 10^8 s^{-1}	–	0.68 ± 0.04	1.2 ± 0.2
PC-N4	CT	Φ_{ISC}	–	–	0.57 ± 0.06
		k_{ISC} / 10^8 s^{-1}	–	–	1.0 ± 0.1
PC-N5	CT	Φ_{ISC}	–	0.14 ± 0.02	–
		k_{ISC} / 10^8 s^{-1}	–	0.08 ± 0.01	–
PC-O1	CT	Φ_{ISC}	0.84 ± 0.21	0.43 ± 0.05	0.56 ± 0.03
		k_{ISC} / 10^8 s^{-1}	4.0 ± 1.0	2.9 ± 0.5	2.3 ± 0.2
PC-O2	CT	Φ_{ISC}	0.74 ± 0.09	0.56 ± 0.03	0.70 ± 0.03
		k_{ISC} / 10^8 s^{-1}	0.9 ± 0.2	0.9 ± 0.1	2.9 ± 0.4
PC-O3	CT	Φ_{ISC}	–	–	–
		k_{ISC} / 10^8 s^{-1}	–	–	–
PC-S	CT	Φ_{ISC}	0.37 ± 0.07	0.63 ± 0.03	0.57 ± 0.05
		k_{ISC} / 10^8 s^{-1}	0.6 ± 0.1	1.7 ± 0.1	3.2 ± 0.3

(a) An entry of – indicates no evidence of T_1-state population, suggesting $\Phi_{ISC} \approx 0$.
(b) Uncertainties are from the fitted errors in the amplitudes of the components of multi-exponential fits to single kinetic data sets.

Intersystem crossing is a minor pathway in the relaxation of most of the photoexcited dihydrophenazine PCs studied, particularly in DCM and DMF.[17] For PC-N5 solution in DCM, we recently reported $\Phi_{ISC} = 0.13 \pm 0.02$, consistent with this general conclusion.[28] The exception is toluene, where three out of the five dihydrophenazine PCs (PC-N2, PC-N3, PC-N4) show significant intersystem crossing efficiencies. PC-N4 in toluene is an interesting case, as in this solvent the greater S_1-state lifetime (5.31 ± 0.17 ns from TCSPC) apparently provides sufficient time for ISC to compete with radiative decay to S_0. In contrast, despite PC-N1 having S_1 lifetimes of several ns in the three solvents (only shortened to ~2 ns in DCM by electron transfer reactions with the solvent), we see no evidence for ISC, indicating weak spin-orbit coupling and/or no accessible regions of near-degeneracy between the singlet and triplet manifolds. Higher triplet-state quantum yields are observed for the phenoxazine and phenothiazine PCs studied, which may reflect the longer S_1 lifetimes of these compounds, as well as the influence of a larger spin-orbit interaction in the sulfur-containing phenothiazine.

Sartor *et al*. recently reported a time-resolved spectroscopy study of four N-aryl phenothiazines with biphenyl core substituents.[10] They showed the importance of singlet states with CT character involving the nearly orthogonal N-aryl group in promoting ISC to a triplet state characterized by partial charge transfer to one biphenyl group. The large change in orbital angular momentum associated with the change in electron density between these nearly orthogonal molecular orbitals of CT character enhances the spin-orbit interaction.[49, 50] ISC quantum yields therefore depended sensitively on the electron-withdrawing character of the N-aryl substituent, and by implication, the choice of solvent because of the influence of solvent polarity on the energies of the CT states. For measurements made in DMAc, their deduced quantum yields Φ_{ISC} were in the range 0.4 – 1.0 for N-phenyl, N-naphthyl and N-fluoro-naphthyl substituents, with the

corresponding k_{ISC} values in DMAc ranging from $(1.0 – 2.0) \times 10^8$ s^{-1}. These values are comparable to those we report for PC-S in Table 5, although the mechanism for ISC explored by Sartor *et al*. requires CT states localized on core substituents such as biphenyl groups and does not apply to PC-S which has no such core substituents. Our measurements across dihydrophenazine, phenoxazine and phenothiazine PCs suggest that CT character is not a pre-requisite for ISC in these classes of compounds because we see triplet-state population growth from S_1 states of both LE and CT character. The ISC rate coefficients are comparable, and both these and Φ_{ISC} values are sensitive to the properties of the solvent, indicating tuning of excited state energies by the environment plays an important role.

d) Structural and solvent effects on excited state lifetimes and electronic properties

In all the dihydrophenazine PCs studied, the S_1-state lifetimes are highly sensitive to the electron withdrawing or donating nature of the N-aryl substituents, as well as to the properties of the solvent. The excited states of the phenoxazine PCs also show sensitivity to these types of structural and environmental change. In DCM solutions, the highly reducing excited states of these PCs facilitate electron transfer reactions with the solvent, but no such reactions shorten the S_1-state lifetimes in DMF and toluene. Instead, the different dielectric constants of the two solvents modify to greater or lesser extents the energies of the CT and LE character excited states, as do the N-aryl substituents. In the cases of PC-N3 and PC-N4, which have electron-withdrawing N-aryl substituents and hence CT-character S_1 states, the effect of solvent is most pronounced. In these two PCs, which are known to exert good control over polymer dispersity in O-ATRP,[6] the S_1 lifetimes in DMF (and DMAc) are less than 1 ns. The likelihood is that the tuning in energy of the CT states by these intramolecular and environmental influences makes efficient pathways for non-

radiative $S_1 \rightarrow S_0$ decay accessible via conical intersections between the electronic states. Further investigation of this supposition requires electronic structure calculations which map the structure and energy dependences of seams of intersection between the excited and ground state potential energy surfaces.

Changes to S_1-state lifetimes have consequences for the quantum yields for ISC, because short-lived S_1 states favour relaxation within the singlet spin manifold over spin-changing dynamics. From a combination of the experimental evidence reported here for dihydrophenazine PC-N1, PC-N3 and PC-N4 photocatalysts, and experimental polymerization studies using these PCs, we suggest that population via ISC of a long-lived triplet state of the optically excited PC is not an essential prerequisite for effective ATRP control of polymer dispersity. These and the other dihydrophenazine compounds show little or no propensity for ISC (Table 5), with the exception of PC-N2 which was reported to be an inferior PC for photoredox catalysed control of polymer dispersity in O-ATRP.[6] PC-N3 shows solvent-dependent ISC quantum yields and rate coefficients, but its S_1 lifetime in DMF is short enough to outcompete ISC. Hence, PC-N3(T_1) is unlikely to play a significant role in radical generation for O-ATRP synthesis in solvents such as DMF and DMAc.

Several photocatalysts based on a phenoxazine core are reported to show strong solvent dependence to their fluorescence spectra, indicating CT character of the emissive S_1 state.[7] Our TVAS and TCSPC data (Table 3) reveal singlet lifetimes of a few ns in the three solvents studied, but also a slower component to the ground-state recovery in two of the chosen phenoxazine PCs, indicating ISC to the triplet manifold of states. Reduction by electron transfer from either the S_1 or T_1 state may therefore contribute to photoredox catalysed O-ATRP activity in these two cases.

Instead of focusing on ISC propensities, we propose that the Gibbs energy change for the electron transfer reaction is an important metric for assessing the efficacy of these PCs in O-ATRP control, as outlined in Marcus theory and suggested in earlier work.[17, 47] This argument is developed further in a companion paper in which supporting evidence is presented from direct measurements of intermolecular electron transfer for the nine PCs studied here. However, we note here that whether electron transfer occurs from the S_1 or T_1 state will influence the Gibbs energy changes and hence ET rate coefficients, and the results presented in this article unravel the PC-structure and solvent-dependent propensities for S_1 population to undergo ISC. The S_1 lifetime also appears to be an important factor for consideration, with consequences both for the propensity for diffusive intermolecular electron transfer and ISC quantum yields. In several of the PCs studied here, and more so for the dihydrophenazine derivatives, S_1-state lifetimes are controlled by non-radiative and radiative relaxation pathways to S_0, not by ISC dynamics to populate T_1.

The sensitivity of the excited-state dynamics of the various PCs to the choice of solvent raises interesting questions about the effects of the environment on PC performance in O-ATRP. Under the types of conditions used for polymer growth, the solvent is typically DMAc or DMF, but the solution also includes a significant fraction of a lower polarity monomer. As our solvent-dependent measurements reported in Tables 2 - 5 show, the local solvation environment of a photoexcited PC in these mixed solutions will affect its S_1-state lifetime and ISC yield.

5. Conclusions

Study of the femtosecond to nanosecond timescale photophysical dynamics of organic molecular photocatalysts is essential to identify the electronic states that underlie their useful photocatalytic properties. We report the lifetimes and relaxation pathways of the excited electronic

states of nine representative molecular photocatalysts for O-ATRP. Time-resolved spectroscopic measurements performed with sub-picosecond time resolution in three solvents (DMF, DCM and toluene) directly explore the states involved in the photoredox behaviour of these compounds. In conjunction with quantum-chemical calculations and global kinetic fitting, the observed spectroscopic features reveal the electronic states populated upon photoexcitation and internal conversion, the efficacies for triplet state branching and ground state recovery, and their dependence on solvent. The results are consolidated with our previous publications on this topic to outline general photophysical principles.[17, 28, 29]

For solutions of dihydrophenazine PCs in DMF, catalysts possessing CT excited-state character have relatively short S_1-state lifetimes (e.g., 136 ps for PC-N3 and 500 ps for PC-N4), whereas those with LE character have longer S_1 lifetimes (e.g., 11 ns for PC-N1 and 17 ns for PC-N2). Experimental results point towards polar solvents shortening the excited state lifetimes, most likely by stabilizing the CT state energies relative to the corresponding ground states and opening non-radiative relaxation pathways via conical intersections. We posit that detailed quantum chemical calculations can help ascertain the state-specific relaxation mechanisms in the future.

The S_1-state lifetimes range from sub-ns to a few tens of ns for all the OPCs studied. ISC is found to be a minor relaxation pathway for PCs with short-lived S_1 states. In these cases, bimolecular, excited-state electron transfer reactions must compete with the (ultra)fast intramolecular energy relaxation timescale if the PCs are to play an effective role in O-ATRP. We propose that rapid loss of the excited state population may be partially compensated for by the high reduction potentials of the excited singlet states, which minimize activation barriers for bimolecular electron-transfer reactions. Crucially, the T_1 state need not be the sole electronic state responsible for electron transfer, as is often assumed in O-ATRP studies.

Evidence for competition between electron-transfer from the S_1 and T_1 states to a radical initiator is presented in a companion paper, in which bimolecular electron transfer rate coefficients are reported for the nine dihydrophenazine, phenoxazine and phenothiazine PCs studied here. The observed trends are discussed in terms of Marcus−Savéant theory, and they indicate that both static and dynamic (diffusional) rate coefficients for the photoinduced electron transfer will be lower from the T_1 than from the S_1 state because of the smaller excited-state reduction potentials. In general, a combination of (i) short, first-excited singlet state lifetimes, (ii) low propensities for intersystem crossing, and (iii) slower photoinduced electron transfer rates are expected to maintain a low steady-state concentration of radical intermediates, thereby exercising a better control on polymer dispersity in O-ATRP reactions. Our spectroscopic data with sub-picosecond time resolution underline the importance of considering both S_1 and T_1 state reduction potentials in assessing the usefulness of organic photocatalysts for ATRP. These results will further guide the design principles and applications of these general and widespread classes of PC compounds.[35, 51, 52]

Acknowledgements

This work was supported by EPSRC grant EP/ R012695/1. The ultrafast laser laboratory at the University of Bristol was established with funding from ERC Advanced Grant CAPRI 290966. MS is supported by Marie Skłodowska-Curie fellowship MARCUS 793799. L.L.B and J.T. thank the Bristol Chemical Synthesis Centre for Doctoral Training, funded by EPSRC (EP/L015366/1), and the University of Bristol, for PhD studentships. G.A. thanks EPSRC for Ph.D. studentship funding through EP/N509619/1. T.A.A.O acknowledges the Royal Society University Research Fellowship UF1402310 and URF\R\201007.

Supporting Information

The Supporting Information contains synthetic methods for preparation of the PCs; selected physical properties of the solvents; steady state fluorescence and FTIR spectra of the organic PCs; analysis of transient electronic absorption spectra of the organic PCs; time-correlated single photon counting (TCSPC) data.

Data Availability

Data are available at the University of Bristol data repository, data.bris at https://doi.org/10.5523/bris.jud6zf0aehpn2pjwv1klmba58.

References

1. Matyjaszewski, K.; Xia, J., Atom Transfer Radical Polymerization. *Chem. Rev.* **2001,** *101*, 2921-2990.
2. Romero, N. A.; Nicewicz, D. A., Organic Photoredox Catalysis. *Chem. Rev.* **2016,** *116*, 10075−10166.
3. Treat, N. J.; Sprafke, H.; Kramer, J. W.; Clark, P. G.; Barton, B. E.; de Alaniz, J. R.; Fors, B. P.; Hawker, C. J., Metal-Free Atom Transfer Radical Polymerization. *J. Am. Chem. Soc.* **2014,** *136*, 16096−16101.
4. Chen, M.; Zhong, M.; Johnson, J. A., Light-Controlled Radical Polymerization: Mechanisms, Methods, and Applications. *Chem. Rev.* **2016,** *116*, 10167−10211.
5. Corrigan, N.; Shanmugam, S.; Xu, J.; Boyer, C., Photocatalysis in Organic and Polymer Synthesis. *Chem. Soc. Rev.* **2016,** *45*, 6165−6212.
6. Theriot, J. C.; Lim, C.-H.; Yang, H.; Ryan, M. D.; Musgrave, C. B.; Miyake, G. M., Organocatalyzed Atom Transfer Radical Polymerization Driven by Visible Light. *Science* **2016,** *352*, 1082-1086.

7. McCarthy, B. G.; Pearson, R. M.; Lim, C.-H.; Sartor, S. M.; Damrauer, N. H.; Miyake, G. M., Structure−Property Relationships for Tailoring Phenoxazines as Reducing Photoredox Catalysts. *J. Am. Chem. Soc.* **2018,** *140*, 5088−5101.
8. Corbin, D. A.; Lim, C.-H.; Miyake, G. M., Phenothiazines, dihydrophenazines, and phenoxazines: sustainable alternatives to precious-metal-based photoredox catalysts. *Aldrichimica Acta* **2019,** *52*, 7 - 21.
9. Discekici, E. H.; Pester, C. W.; Treat, N. J.; Lawrence, J.; Mattson, K. M.; Narupai, B.; Toumayan, E. P.; Luo, Y.; McGrath, A. J.; Clark, P. G.; Read de Alaniz, J.; Hawker, C. J., Simple Benchtop Approach to Polymer Brush Nanostructures Using Visible-Light-Mediated Metal-Free Atom Transfer Radical Polymerization. *ACS Macro Lett.* **2016,** *5*, 258−262.
10. Sartor, S. M.; Chrisman, C. H.; Pearson, R. M.; Miyake, G. M.; Damrauer, N. H., Designing High-Triplet-Yield Phenothiazine Donor−Acceptor Complexes for Photoredox Catalysis. *J. Phys. Chem. A* **2020,** *124*, 817−823.
11. Sartor, S. M.; McCarthy, B. G.; Pearson, R. M.; Miyake, G. M.; Damrauer, N. H., Exploiting Charge-Transfer States for Maximizing Intersystem Crossing Yields in Organic Photoredox Catalysts. *J. Am. Chem. Soc.* **2018,** *140*, 4778−4781.
12. Prier, C. K.; Rankic, D. A.; MacMillan, D. W. C., Visible Light Photoredox Catalysis with Transition Metal Complexes: Applications in Organic Synthesis. *Chem. Rev.* **2013,** *113*, 5322−5363.
13. Jockusch, S.; Yagci, Y., The Active Role of Excited States of Phenothiazines in Photoinduced Metal Free Atom Transfer Radical Polymerization: Singlet or Triplet Excited States? *Polymer Chem.* **2016,** *7*, 6039-6043.
14. Bressler, C.; Milne, C.; Pham, V.-T.; ElNahhas, A.; van der Veen, R. M.; Gawelda, W.; Johnson, S.; Beaud, P.; Grolimund, D.; Kaiser, M.; Borca, C. N.; Ingold, G.; Abela, R.; Chergui, M., Femtosecond XANES Study of the Light-Induced Spin Crossover Dynamics in an Iron(II) Complex. *Science* **2009,** *323*, 489-492.
15. Auböck, G.; Chergui, M., Sub-50-fs Photoinduced Spin Crossover in [Fe(bpy)3]2+. *Nat. Chem.* **2015,** *7*, 629-633.

16. Monnia, R.; Capanoa, G.; Auböcka, G.; Gray, H. B.; Vlcek, A.; Tavernellie, I.; Chergui, M., Vibrational Coherence Transfer in the Ultrafast Intersystem Crossing of a Diplatinum Complex in Solution. *Proc. Nat. Acad. Sci.* **2018,** *115*, 6396-6403.
17. Koyama, D.; Dale, H. J. A.; Orr-Ewing, A. J., Ultrafast Observation of a Photoredox Reaction Mechanism: Photoinitiation in Organocatalyzed Atom-Transfer Radical Polymerization. *J. Am. Chem. Soc.* **2018,** *140*, 1285−1293.
18. Noto, N.; Takahashi, K.; Goryo, S.; Takakado, A.; Iwata, K.; Koike, T.; Akita, M., Laser Flash Photolysis Studies on Radical Monofluoromethylation by (Diarylamino)naphthalene Photoredox Catalysis: Long Lifetime of the Excited State is Not Always a Requisite. *J. Org. Chem.* **2020,** *85*, 13220-13227.
19. Ryan, M. D.; Theriot, J. C.; Lim, C.-H.; Yang, H.; Lockwood, A. G.; Garrison, N. G.; Lincoln, S. R.; Musgrave, C. B.; Miyake, G. M., Solvent Effects on the Intramolecular Charge Transfer Character of N,N-Diaryl Dihydrophenazine Catalysts for Organocatalyzed Atom Transfer Radical Polymerization *J. Polym. Sci., Part A: Polym. Chem.* **2017,** *55*, 3017−3027.
20. Lim, C.-H.; Ryan, M. D.; McCarthy, B. G.; Theriot, J. C.; Sartor, S. M.; Damrauer, N. H.; Musgrave, C. B.; Miyake, G. M., Intramolecular Charge Transfer and Ion Pairing in N,N-Diaryl Dihydrophenazine Photoredox Catalysts for Efficient Organocatalyzed Atom Transfer Radical Polymerization. *J. Am. Chem. Soc.* **2017,** *139*, 348−355.
21. Pearson, R. M.; Lim, C.-H.; McCarthy, B. G.; Musgrave, C. B.; Miyake, G. M., Organocatalyzed Atom Transfer Radical Polymerization Using N-Aryl Phenoxazines as Photoredox Catalysts. *J. Am. Chem. Soc.* **2014,** *136*, 16096−16101.
22. Dadashi-Silab, S.; Pan, X.; Matyjaszewski, K., Phenyl Benzo[b]phenothiazine as a Visible Light Photoredox Catalyst for Metal-Free Atom Transfer Radical Polymerization. *Chem. Eur. J.* **2017,** *23*, 5972 – 5977.
23. Miyake, G. M.; Theriot, J. C., Perylene as an Organic Photocatalyst for the Radical Polymerization of Functionalized Vinyl Monomers through Oxidative Quenching with Alkyl Bromides and Visible Light. *Macromol.* **2014,** *47*, 8255-8261.
24. Sartor, S. M.; Lattke, Y. M.; McCarthy, B. G.; Miyake, G. M.; Damrauer, N. H., Effects of Naphthyl Connectivity on the Photophysics of Compact Organic Charge-Transfer Photoredox Catalysts. *J. Phys. Chem. A* **2019,** *123*, 4727−4736.

25. Wang, J.-S.; Matyjaszewski, K., Controlled/"Living" Radical Polymerization. Atom Transfer Radical Polymerization in the Presence of Transition-Metal Complexes. *J. Am. Chem. Soc.* **1995,** *117*, 5614-5615.
26. Rolland, M.; Whitfield, R.; Messmer, D.; Parkatzidis, K.; Truong, N. P.; Anastasaki, A., Effect of Polymerization Components on Oxygen-Tolerant Photo-ATRP. *ACS Macro Lett.* **2019,** *8*, 1546-1551.
27. Martinez, M. R.; Sobieski, J.; Lorandi, F.; Fantin, M.; Dadashi-Silab, S.; Xie, G.; Olszewski, M.; Pan, X.; Ribelli, T. G.; Matyjaszewski, K., Understanding the Relationship between Catalytic Activity and Termination in PhotoATRP: Synthesis of Linear and Bottlebrush Polyacrylates. *Macromol.* **2020,** *53*, 59-67.
28. Lewis-Borrell, L.; Sneha, M.; Bhattacherjee, A.; Clark, I. P.; Orr-Ewing, A. J., Mapping the Multi-Step Mechanism of a Photoredox Catalyzed Atom-Transfer Radical Polymerization Reaction by Direct Observation of the Reactive Intermediates. *Chem. Sci.* **2020,** *11*, 4475-4481.
29. Sneha, M.; Lewis-Borrell, L. J.; Shchepanovska, D.; Bhattacherjee, A.; Tyler, J. L.; Orr-Ewing, A. J., Solvent-Dependent Photochemical Dynamics of a Phenoxazine-Based Photoredox Catalyst. *Z. Phys. Chem.* **2020,** *234*, 1475 – 1494
30. Pan, X.; Lamson, M.; Yan, J.; Matyjaszewski, K., Photoinduced Metal-Free Atom Transfer Radical Polymerization of Acrylonitrile. *ACS Macro Lett.* **2015,** *4*, 192-196.
31. Bhattacherjee, A.; Sneha, M.; Lewis-Borrell, L.; Tau, O.; Clark, I. P.; Orr-Ewing, A. J., Picosecond to Millisecond Tracking of a Photocatalytic Decarboxylation Reaction Provides Direct Mechanistic insights. *Nat. Commun.* **2019,** *10*, 5152.
32. Roberts, G. M.; Marroux, H. J. B.; Grubb, M. P.; Ashfold, M. N. R.; Orr-Ewing, A. J., On the Participation of Photoinduced N-H Bond Fission in Aqueous Adenine at 266 and 220 nm: a Combined Ultrafast Transient Electronic and Vibrational Absorption Spectroscopy Study. *J. Phys. Chem. A* **2014,** *118*, 11211–11225.
33. Greetham, G. M.; Donaldson, P. M.; Nation, C.; Sazanovich, I. V.; Clark, I. P.; Shaw, D. J.; Parker, A. W.; Towrie, M., A 100 kHz Time-Resolved Multiple-Probe Femtosecond to Second Infrared Absorption Spectrometer. *Appl. Spectrosc.* **2016,** *70*, 645–653.

34. Koyama, D.; Donaldson, P. M.; Orr-Ewing, A. J., Femtosecond to Microsecond Observation of the Photochemical Reaction of 1,2-Di(quinolin-2-yl)disulphide with Methyl Methacrylate. *Phys. Chem. Chem. Phys.* **2017,** *19*, 12981-12991.
35. Orr-Ewing, A. J., How can Ultrafast Laser Spectroscopy Inform the Design of New Organic Photoredox Catalysts for Chemical and Materials Synthesis? . *Struct. Dyn.* **2019,** *6*, 010901.
36. Frisch, M. J.; Trucks, G. W.; Schlegel, H. B.; Scuseria, G. E.; Robb, M. A.; Cheeseman, J. R.; Scalmani, G.; Barone, V.; Mennucci, B.; Petersson, G. A.; Nakatsuji, H.; Caricato, M.; Li, X.; Hratchian, H. P.; Izmaylov, A. F.; Bloino, J.; Zheng, G.; Sonnenberg, J. L.; Hada, M.; Ehara, M.; Toyota, K.; Fukuda, R.; Hasegawa, J.; Ishida, M.; Nakajima, T.; Honda, Y.; Kitao, O.; Nakai, H.; Vreven, T.; Montgomery, J. A.; Peralta, J. E.; Ogliaro, F.; Bearpark, M. J.; Heyd, J. J.; Brothers, E.; Kudin, K. N.; Staroverov, V. N.; Kobayashi, R.; Normand, J.; Raghavachari, K.; Rendell, A.; Burant, J. C.; Iyengar, S. S.; Tomasi, J.; Cossi, M.; Rega, N.; Millam, J. M.; Klene, M.; Knox, J. E.; Cross, J. B.; Bakken, V.; Adamo, C.; Jaramillo, J.; Gomperts, R.; Stratmann, R. E.; Yazyev, O.; Austin, A. J.; Cammi, R.; Pomelli, C.; Ochterski, J. W.; Martin, R. L.; Morokuma, K.; Zakrzewski, V. G.; Voth, G. A.; Salvador, P.; Dannenberg, J. J.; Dapprich, S.; Daniels, A. D.; Farkas, O.; Foresman, J. B.; Ortiz, J. V.; Cioslowski, J.; Fox, D. J. *Gaussian 09*, Gaussian Inc., Wallingford CT, 2009.
37. Marenich, A. V.; Cramer, C. J.; Truhlar, D. G., Universal Solvation Model Based on Solute Electron Density and on a Continuum Model of the Solvent Defined by the Bulk Dielectric Constant and Atomic Surface Tensions. *J. Phys. Chem. B* **2009,** *113*, 6378-6396.
38. Miertuš, S.; Scrocco, E.; Tomasi, J., Electrostatic Interaction of a Solute with a Continuum. A Direct Utilizaion of Ab Initio Molecular Potentials for the Prevision of Solvent Effects. *Chem. Phys.* **1981,** *55*, 117-129.
39. Tomasi, J.; Mennucci, B.; Cammi, R., Quantum Mechanical Continuum Solvation Models. *Chem. Rev.* **2005,** *105*, 2999-3094.
40. Goerigk, L.; Grimme, S., Efficient and Accurate Double-Hybrid-Meta-GGA Density Functionals—Evaluation with the Extended GMTKN30 Database for General Main Group Thermochemistry, Kinetics, and Noncovalent Interactions. *J. Chem. Theor. Comp.* **2011,** *7*, 291-309.

41. Grimme, S.; Antony, J.; Ehrlich, S.; Krieg, H., A Consistent and Accurate Ab Initio Parametrization of Density Functional Dispersion Correction (DFT-D) for the 94 Elements H-Pu. *J. Chem. Phys.* **2010,** *132*, 154104.
42. Yanai, T.; Tew, D. P.; Handy, N. C., A New Hybrid Exchange–Correlation Functional using the Coulomb-Attenuating Method (CAM-B3LYP). *Chem. Phys. Lett.* **2004,** *393*, 51-57.
43. Peach, M. J. G.; Benfield, P.; Helgaker, T.; Tozer, D. J., Excitation Energies in Density Functional Theory: An Evaluation and a Diagnostic Test. *J. Chem. Phys.* **2008,** *128*, 044118.
44. Chaudhuri, S.; Rudshteyn, B.; Prémont-Schwarz, M.; Pines, D.; Pines, E.; Huppert, D.; Nibbering, E. T. J.; Batista, V. S., Ultrafast Photo-Induced Charge Transfer of 1-Naphthol and 2-Naphthol to Halocarbon Solvents. *Chem. Phys. Lett.* **2017,** *683*, 49–56.
45. Grubb, M. P.; Orr-Ewing, A. J.; Ashfold, M. N. R., KOALA: a Program for the Processing and Decomposition of Transient Spectra. *Rev. Sci. Instrumen.* **2014,** *85*, 064104.
46. Turro, N. J.; Ramamurthy, V.; Scaiano, J. C., Modern Molecular Photochemistry of Organic Molecules. *University Science Books: Mill Valley, CA* **2010**.
47. Pan, X.; Fang, C.; Fantin, M.; Malhotra, N.; So, W. Y.; Peteanu, L. A.; Isse, A. A.; Gennaro, A.; Liu, P.; Matyjaszewski, K., Mechanism of Photoinduced Metal-Free Atom Transfer Radical Polymerization: Experimental and Computational Studies. *J. Am. Chem. Soc.* **2016,** *138*, 2411−2425.
48. Theriot, J. C.; McCarthy, B. G.; Lim, C.-H.; Miyake, G. M., Organocatalyzed Atom Transfer Radical Polymerization: Perspectives on Catalyst Design and Performance. *Macromol. Rapid Commun.* **2017,** *38*, 1700040.
49. Benniston, A. C.; Harriman, A.; Li, P.; Rostron, J. P.; van Ramesdonk, H. J.; Groeneveld, M. M.; Zhang, H.; Verhoeven, J. W., Charge Shift and Triplet State Formation in the 9-Mesityl-10-methylacridinium Cation. *J. Am. Chem. Soc.* **2005,** *127*, 16054-16064.
50. Dance, Z. E. X.; Mickley, S. M.; Wilson, T. M.; Ricks, A. B.; Scott, A. M.; Ratner, M. A.; Wasielewski, M. R., Intersystem Crossing Mediated by Photoinduced Intramolecular Charge Transfer: Julolidine−Anthracene Molecules with Perpendicular π Systems. *J. Phys. Chem. A* **2008,** *112*, 4194-4201.

51. Enciso, A. E.; Fu, L.; Russell, A. J.; Matyjaszewski, K., A Breathing Atom-Transfer Radical Polymerization: Fully Oxygen-Tolerant Polymerization Inspired by Aerobic Respiration of Cells. *Angew. Chem. Int. Ed.* **2018,** *57*, 933-936.
52. Luca Buzzetti, L.; Crisenza, G. E. M.; Melchiorre, P., Mechanistic Studies in Photocatalysis. *Angew. Chem. Int. Ed.* **2019,** *58*, 3730-3747.

TOC Graphic

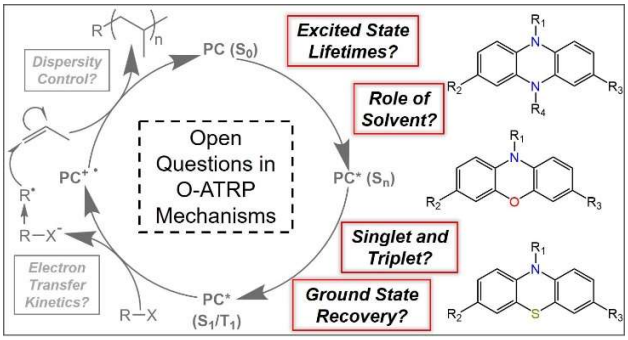
Dispersity Control?
PC (S0)
Excited State Lifetimes?
Role of Solvent?
Open Questions in O-ATRP Mechanisms
PC+ •
PC* (Sn)
R•
R—X-
Singlet and Triplet?
Electron Transfer Kinetics?
R—X
PC* (S1/T1)
Ground State Recovery?